REPORT NO.
UCB/SEMM-90/13

STRUCTURAL ENGINEERING,
MECHANICS AND MATERIALS

MIXED FORMULATIONS FOR PLATE BENDING ELEMENTS

by

SHMUEL L. WEISSMAN

and

ROBERT L. TAYLOR

JULY 1990

DEPARTMENT OF CIVIL ENGINEERING
UNIVERSITY OF CALIFORNIA
BERKELEY, CALIFORNIA

MIXED FORMULATIONS FOR PLATE BENDING ELEMENTS

Shmuel L. Weissman & Robert L. Taylor

Department of Civil Engineering
University of California at Berkeley

ABSTRACT

Plate bending elements, based upon the Reissner-Mindlin plate theory, are formulated via the Hu-Washizu variational principle, including the Hellinger-Reissner functional as a special case. It is proven that these elements avoid the well-known shear locking behavior at the thin plate limit. To obtain this objective, the assumed stress and strain fields are constructed to satisfy *a priori* the homogeneous equilibrium equations in a weak sense. The proposed elements are shown to perform well on a set of standard problems.

CONTENT

MIXED FORMULATIONS FOR PLATE BENDING ELEMENTS

Shmuel L. Weissman & Robert L. Taylor

Department of Civil Engineering
University of California at Berkeley

1. INTRODUCTION

Plate bending elements, based upon the Reissner-Mindlin plate theory (Reissner [1945] and Mindlin [1951]), are formulated within the framework of the Hu-Washizu variational principle (Washizu [1948]), including the Hellinger-Reissner variational principle as a special case. The method proposed by Weissman & Taylor [1990b] is used to generate the assumed stress and strain fields. The objective of this work is to show that a systematic development of elements that avoid shear locking at the element level is possible. Proving that the proposed formulation leads to such elements is the main contribution of this paper.

A major difficulty in the development of plate bending elements based on theories that account for shear deformations, such as the Reissner-Mindlin theory, is the locking behavior exhibited at the thin plate limit. This phenomenon is attributed to the failure of the numerical approximation to enforce the internal constraint, which is the ratio of transverse shear strain to curvature going to zero as the plate thickness is reduced to zero.

Much research has been directed at overcoming the locking behavior at the thin plate limit (see Hughes [1987] and references therein). A cornerstone in the development of many of the recently proposed elements (e.g., Tezduyar & Hughes [1981], Bathe & Dvorkin [1985], and Zienkiewicz, *et al.* [1989]) is the constraint count method (see Hughes [1987]). The underlying idea behind this approach is that locking behavior can be avoided if the number of constraints is smaller then the number of active equations. To obtain the "right" number of constraints, these elements resort to sharing constraints across element boundaries. Consequently, shear locking is avoided at the system level, but not at the element level.

Finite element approximations of problems involving internal constraints often result in locking. This difficulty was put in the form of a limitation principle by Fraeijs de Veubeke [1965]. In order to avoid this limitation principle, the assumed stress and strain fields must satisfy *a priori* the equilibrium equations and thus, effectively satisfy the internal constraints. In the context of finite element methods this requirement can be relaxed, and the equilibrium equations can be satisfied in a weak sense.

Taking advantage of this observation, Weissman & Taylor [1990a] developed plate bending elements via the Hellinger-Reissner functional. Following Pian & Sumihara [1984], the assumed stress field is constructed to satisfy the homogeneous equilibrium equations in a weak sense, relative to a set of incompatible displacements. Consequently, the assumed transverse shear resultant field is coupled into the assumed moment field. It is proven that as a result of this coupling shear locking is avoided at the element level.

A general method to generate assumed stress and strain fields, in the context of the Hu-Washizu functional, is proposed in Weissman & Taylor [1990b]. The key idea is the assumption that the strain field is the sum of two independent fields, termed "compatible" and "incompatible" strain fields. The incompatible strain field is obtained from a set of displacements not contained in the finite element approximation of the displacement solution space (this requirement is crucial to the stability of the resulting elements). To obtain the desired fields the internal energy resulting from the product of the incompatible strain and either the compatible strain or the stress fields is constrained to vanish in a weak sense. The resulting approximation of the stress and compatible strain fields satisfy the homogeneous equilibrium equations in a weak sense and consequently also the internal constraints. Furthermore, the incompatible strain vanishes pointwise at the solution.

The organization of the paper follows. The strong, or classical, form of the Reissner-Mindlin plate bending theory is summarized in Section 2. Element formulation via the Hu-Washizu functional (in resultant form), including stress and strain fields generation, is presented in Section 3. In Section 4 it is proven that the formulation presented in Section 3 leads to elements that avoid shear locking at the element level. The initially assumed stress and strain fields as well as the assumed displacement field are stated in Section 5. Numerical results are contained in Section 6. Concluding remarks are given in Section 7.

2. STRONG FORM

A plate bending theory that accounts for shear deformations, commonly referred to as the Reissner-Mindlin theory, is summarized in this section. It must be pointed out that the stress distribution employed by Reissner accounts for warping of transverse fibers. In this work the effect of warping is neglected. However, a shear correction factor is introduced to compensate for the lack of warping.

Throughout this work, Greek subscripts take the values 1 and 2, while Latin subscripts take the values 1, 2, and 3. Repeated indices imply the usual summation convention. All quantities are referred to a fixed system of rectangular, Cartesian coordinates. A general point in this system is denoted by (x_1, x_2, x_3).

A plate is a three-dimensional body embedded in an Euclidian three-space $\mathbf{R}^3$. In the undeformed configuration the plate domain Ω is of the following form:

$$\Omega := \left\{ \left(x_1, x_2, x_3\right) \in \mathbf{R}^3 \mid x_3 \in \left[\frac{-h(x_1,x_2)}{2}, \frac{h(x_1,x_2)}{2} \right], \left(x_1, x_2\right) \in A \subset \mathbf{R}^2 \right\}$$

where $h(x_1,x_2)$ is the plate thickness and A is a closed region in the $x_1 \times x_2$ plane, bounded by a simple closed curve C. Let C_U and C_t be subregions of C such that $\overline{C_U \bigcup C_t} = C$ and $C_U \bigcap C_t = \phi$, where C_U is the part of C on which displacements are specified and C_t is the part of C on which tractions are specified. h is assumed to be small in comparison to a characteristic length of A. The plane $x_3 = 0$ is denoted the mid-surface of the plate. The outward normal unit vector to C in the $x_1 \times x_2$ plane has the components n_α, and the counterclockwise tangential unit vector has the components t_α.

Following Mindlin [1951], the assumed displacement field is taken as:

$$u_\alpha(x_1,x_2,x_3) := x_3 e_{\alpha\beta}\theta_\beta(x_1,x_2) \tag{2.1a}$$

and

$$u_3(x_1,x_2,x_3) := w\,(x_1,x_2) \tag{2.1.b}$$

where the sign conventions for the rotations are shown in Figure 2.1, and $e_{\alpha\beta}$ are the components of the alternator tensor, given in matrix notation by:

$$\mathbf{e} := \left[e_{\alpha\beta}\right] = \begin{bmatrix} 0 & 1 \\ -1 & 0 \end{bmatrix} \tag{2.2}$$

REMARK: Equations (2.1) are equivalent to the following statements:

i A straight fiber normal to the mid-surface in the reference configuration remains straight but not necessarily normal to the mid-surface in the deformed configuration, and

ii the transverse displacement, w, does not vary through the thickness. ▪

In view of the assumed displacement field, equations (2.1), the strain field is given by:

$$\gamma_\alpha = 2\epsilon_{\alpha 3} = 2\epsilon_{3\alpha} = e_{\alpha\beta}\theta_\beta + w_{,\alpha} \tag{2.3a}$$

and

$$\epsilon_{\alpha\beta} = x_3 \kappa_{\alpha\beta} = \frac{1}{2} x_3 \left(e_{\alpha\gamma}\theta_{\gamma,\beta} + e_{\beta\gamma}\theta_{\gamma,\beta}\right) \tag{2.3b}$$

where γ is the transverse shear strain vector, and κ is the curvature tensor. In matrix

notation, equations (2.3) are given by:

$$\gamma = \mathbf{L}^s \mathbf{U} \tag{2.4a}$$

and

$$\kappa = \mathbf{L}^b \mathbf{U} \tag{2.4b}$$

where $\mathbf{U}^T := \left[w, \theta_1, \theta_2 \right]$ is the displacement vector; $\mathbf{L}^b$ is the curvature displacement operator, given by:

$$\mathbf{L}^b := \begin{bmatrix} 0 & 0 & -\frac{\partial}{\partial x_1} \\ 0 & \frac{\partial}{\partial x_2} & 0 \\ 0 & \frac{\partial}{\partial x_1} & -\frac{\partial}{\partial x_2} \end{bmatrix} \tag{2.5}$$

and $\mathbf{L}^s$ is the transverse shear strain displacement operator, given by:

$$\mathbf{L}^s := \begin{bmatrix} \frac{\partial}{\partial x_1} & 0 & 1 \\ \frac{\partial}{\partial x_2} & -1 & 0 \end{bmatrix} \tag{2.6}$$

Plate kinematics are summarized in Figure 2.2.

The stress resultants are defined as:

$$Q_\alpha := \int_{\frac{-h}{2}}^{\frac{h}{2}} \sigma_{3\alpha}\, dx_3 \qquad \text{Shear resultants.}$$

$$M_{\alpha\beta} := \int_{\frac{-h}{2}}^{\frac{h}{2}} \sigma_{\alpha\beta} x_3 dx_3 \qquad \text{Moment resultants.}$$

Sign conventions for transverse shear and moment resultants are given in Figure 2.3.

The distributed loads are defined as:

$$\bar{Q} := \sigma_{33} \Big|_{\frac{-h}{2}}^{\frac{h}{2}} + \int_{\frac{-h}{2}}^{\frac{h}{2}} b_3\, dx_3 \qquad \text{Transverse load.}$$

$$\bar{M}_\alpha := \sigma_{\alpha 3} x_3 \Big|_{\frac{-h}{2}}^{\frac{h}{2}} + \int_{\frac{-h}{2}}^{\frac{h}{2}} b_\alpha x_3\, dx_3 \qquad \text{Couple loads.}$$

where $\mathbf{b}$ is the body force vector.

In order to define the boundary conditions, the following definitions are introduced:

$M_n := n_\alpha n_\beta M_{\alpha\beta}$ Normal bending moment.

$M_{nt} := n_\alpha t_\beta M_{\alpha\beta}$ Twist moment.

$Q_n := n_\alpha Q_\alpha$ Normal shear.

The equilibrium equations can be deduced from the three-dimensional ones, and are given by:

$$div\mathbf{M} - \mathbf{Q} + \bar{\mathbf{M}} = \mathbf{0} \tag{2.7a}$$

and

$$div\mathbf{Q} + \bar{Q} = 0 \tag{2.7b}$$

The constitutive equations can be derived from the three-dimensional constitutive relations. Plane stress hypothesis is a good approximation of the stresses in thin plates. Consequently, σ_{33} is assumed to be zero everywhere in Ω. $\sigma_{\alpha 3}$, on the other hand, are needed to maintain equilibrium in the x_3 direction and thus, cannot be neglected. The constitutive equations, in matrix notation, are given by:

$$\mathbf{M} = \mathbf{D}^b \kappa \tag{2.8a}$$

and

$$\mathbf{Q} = \alpha \mathbf{D}^s \gamma \tag{2.8b}$$

where $\mathbf{D}^b$ is the elastic coefficients matrix, given in terms of Young's modulus, E, and Poisson's ratio, ν, by:

$$\mathbf{D}^b = \frac{E h^3}{12(1-\nu^2)} \begin{bmatrix} 1 & \nu & 0 \\ \nu & 1 & 0 \\ 0 & 0 & \frac{1}{2}(1-\nu) \end{bmatrix} \tag{2.9}$$

$\mathbf{D}^s$ is the transverse shear elastic coefficient matrix, given by:

$$\mathbf{D}^s = \frac{E h}{2(1+\nu)} \begin{bmatrix} 1 & 0 \\ 0 & 1 \end{bmatrix} \tag{2.10}$$

and α is a correction factor introduced in order to obtain consistent results with the three-dimensional theory, in which the transverse shear varies quadratically along fibers normal to the mid-surface, usually $\alpha = \frac{5}{6}$.

Let the superscript "a" denote prescribed boundary conditions (e.g., Q_n^a is the applied transverse shear). The formal statement of the strong form for the plate bending

boundary value problem is summarized in Box 2.1.

Box 2.1: Plate Bending - Strong Form

Given $\bar{M}_\alpha$, $\bar{Q}$, M_n^a, M_{nt}^a, Q_n^a, W^a, θ_n^a and θ_t^a; find w, θ_α, Q_α and $M_{\alpha\beta}$ such that:

$$
\text{in } A \begin{cases}
div\, \mathbf{M} - \mathbf{Q} + \bar{\mathbf{M}} = \mathbf{0} \\
div\, \mathbf{Q} + \bar{Q} = 0 \\
\mathbf{M} = \mathbf{D}^b\, \boldsymbol{\kappa} \\
\mathbf{Q} = \alpha\, \mathbf{D}^s\, \boldsymbol{\gamma} \\
\kappa_{\alpha\beta} = -\frac{1}{2}\left(e_{\alpha\gamma}\,\theta_{\gamma,\beta} + e_{\beta\gamma}\,\theta_{\gamma,\alpha}\right) \\
\gamma_\alpha = e_{\alpha\beta}\,\theta_\beta + w_{,\alpha}
\end{cases}
$$

$$
\text{on } C_U \begin{cases}
\theta_\alpha = \theta_\alpha^a \\
w = W^a
\end{cases}
$$

$$
\text{on } C_t \begin{cases}
M_n = M_n^a \\
M_{nt} = M_{nt}^a \\
Q_n = Q_n^a
\end{cases}
$$

3. MIXED FORMULATIONS

The weak form counterpart of the strong form presented in Section 2 is derived from the Hu-Washizu functional in Section 3.1. The finite element model is obtained by approximating the assumed fields in Section 3.2. A major difficulty in the development of plate bending elements is the well known locking behavior at the thin plate limit. To avoid this problem, the stress and strain fields are constructed to satisfy *a priori*, in a weak

sense, the homogeneous equilibrium equations.

3.1 Weak Form

The Hu-Washizu functional involves three independent fields: displacement, stress, and strain. However, as the plate bending problem is formulated in terms of resultants, it is more convenient to discuss the stress resultants (i.e., moment and transverse shear) as the independent stress fields, and their conjugate curvature and transverse shear strain as the independent strain fields. In order to proceed with the development it is useful to impose a structure on the spaces of admissible functions. To this end, let the following classes of functions be introduced:

Trial displacement solutions:[1]

$$U := \left\{ \mathbf{U} \mid \mathbf{U} \in H^1(\bar{\Omega}), \mathbf{U} = \mathbf{U}^a \text{ on } C_U \right\}. \tag{3.1}$$

Trial displacement weight functions:

$$W := \left\{ \mathbf{U} \mid \mathbf{U} \in H^1(\bar{\Omega}), \mathbf{U} = \mathbf{0} \text{ on } C_U \right\}. \tag{3.2}$$

Trial moment solutions:

$$M := \left\{ \mathbf{M} \mid \mathbf{M} \in H^0(\bar{\Omega}) \right\} \tag{3.3}$$

Trial transverse shear resultant solutions:

$$Q := \left\{ \mathbf{Q} \mid \mathbf{Q} \in H^0(\bar{\Omega}) \right\} \tag{3.4}$$

Trial curvature solutions:

$$\kappa := \left\{ \kappa \mid \kappa \in H^0(\bar{\Omega}) \right\} \tag{3.5}$$

and trial transverse shear strain solutions:

$$\gamma := \left\{ \gamma \mid \gamma \in H^0(\bar{\Omega}) \right\} \tag{3.6}$$

[1] A function G is said to be a member of H^n if the function and its first n derivatives are members of L_2. A function F is said to be a member of L_2 if it is square integrable, i.e., $\int_\Omega F^2 \, d\Omega < \infty$ where Ω is the domain of interest. Thus, $H^0 = L_2$.

Remark: Since no constraints are imposed on the trial solution spaces used for the stress resultants and strain fields, they can also be used as the trial weight functions for strain and stress resultant fields, respectively. This is possible since the traction boundary conditions evolve naturally from the weak form (see below), and there are no boundary conditions for the strain fields. ▪

The Hu-Washizu functional, stated in resultant form, for the case of plate bending is given by:

$$\Pi_{HW}(\mathbf{M},\mathbf{Q},\kappa,\gamma,\mathbf{U}) := \int_A \left[\frac{1}{2}(\kappa^T \mathbf{D}^b \kappa + \gamma^T \mathbf{D}^s \gamma) + \mathbf{Q}^T(\mathbf{L}^s\mathbf{U} - \gamma) + \mathbf{M}^T(\mathbf{L}^b\mathbf{U} - \kappa) - \mathbf{U}^T\mathbf{F} \right] dA - \int_{C_t} \mathbf{U}^T \mathbf{t}\, d\Gamma \tag{3.7}$$

where $\mathbf{F}^T = \left[\bar{Q}, \bar{M}_1, \bar{M}_2 \right]$ is the body resultant vector, and $\mathbf{t}^T = \left[\bar{Q}_n^a, \bar{M}_n^a, \bar{M}_{nt}^a \right]$ is the applied boundary traction vector.

The weak, or variational, form of the problem may be obtained from the energy functional, Π_{HW}, by making it stationary (i.e., equating the first total variation, of Π_{HW}, to zero). The formal statement of the weak form is stated in Box 3.1.

Box 3.1: Weak Form

Given $\bar{\mathbf{M}}$, $\bar{Q}$, M_n^a, M_{nt}^a, $\mathbf{Q}^a$, and $\mathbf{U}^a$; find $\mathbf{U} \in \boldsymbol{U}$, $\mathbf{M} \in \boldsymbol{M}$, $\mathbf{Q} \in \boldsymbol{Q}$, $\kappa \in \boldsymbol{\kappa}$, and $\gamma \in \boldsymbol{\gamma}$ such that for every $\delta\mathbf{U} \in \boldsymbol{W}$, $\delta\mathbf{M} \in \boldsymbol{M}$, $\delta\mathbf{Q} \in \boldsymbol{Q}$, $\delta\kappa \in \boldsymbol{\kappa}$, and $\delta\gamma \in \boldsymbol{\gamma}$

$$\begin{aligned} 0 = &\int_A \delta\mathbf{M}^T(\mathbf{L}^b\mathbf{U} - \kappa)\, dA + \int_A \delta\mathbf{Q}^T(\mathbf{L}^s\mathbf{U} - \gamma)\, dA \\ &+ \int_A \delta\kappa^T(\mathbf{D}^b\kappa - \mathbf{M})\, dA + \int_A \delta\gamma^T(\mathbf{D}^s\gamma - \mathbf{Q})\, dA \\ &+ \int_A (\mathbf{L}^b\delta\mathbf{U})^T\mathbf{M}\, dA + \int_A (\mathbf{L}^s\delta\mathbf{U})^T\mathbf{Q}\, dA - \int_A \delta\mathbf{U}^T\mathbf{F}\, dA - \int_{C_t} \delta\mathbf{U}^T\mathbf{t}\, d\Gamma \end{aligned}$$

Since $\delta\mathbf{M}$, $\delta\mathbf{Q}$, $\delta\kappa$, $\delta\gamma$, and $\delta\mathbf{U}$ are independent of each other, the weak form is made of five independent equations, known as the Euler-Lagrange equations. The first two equations relate the assumed independent strain field to the displacement field; the third and fourth are the constitutive equations for the plate bending boundary-value problem; the last line, after integration by parts, provide the balance of momentum equations for the plate bending problem.

3.2 Finite Element Approximation

Let the finite element approximating spaces (i.e., finite dimensional subspaces of the trial solution and weight spaces introduced above) be denoted by a superscript "h" (e.g., $\mathbf{U}^h \subset U$). In addition, in anticipation of the development requirements, let the assumed strain fields be decomposed into the additive sum of two independent fields, as follows:

$$\kappa := \kappa^h + \kappa^i \quad \text{and} \quad \gamma := \gamma^h + \gamma^i \tag{3.8}$$

Furthermore, let κ^i and γ^i be given by:

$$\kappa^i := \mathbf{L}^b\, \mathbf{U}^i \quad \text{and} \quad \gamma^i := \mathbf{L}^s\, \mathbf{U}^i \tag{3.9}$$

respectively, where $\mathbf{U}^i$ is a displacement field not contained in $\mathbf{U}^h$ ($\mathbf{U}^i$ is commonly termed incompatible displacements). This constraint on $\mathbf{U}^i$, as will be shown, is crucial to the stability of the resulting elements.

As was pointed out above, the assumed fields must *a priori* satisfy, in a weak sense, the equilibrium equations to avoid shear locking. The approximating stress and strain fields can be constructed to satisfy *a priori* the homgeneous equilibrium equations by introducing the following constraint equations:

$$\int_A \left[\mathbf{M}^{hT}\, \kappa^i + \mathbf{Q}^{hT}\, \gamma^i \right] dA = 0 \tag{3.10a}$$

and

$$\int_A \left[\kappa^{hT}\, \mathbf{D}^b\, \kappa^i + \gamma^{hT}\, \mathbf{D}^s\, \gamma^i \right] dA = 0 \tag{3.10b}$$

Taking the first variation of the energy functional, Π_{HW}, with respect to κ^i, and taking notice of equations (3.10) yields:

$$D\, \Pi_{HW} \cdot \delta\kappa^i = \int_A \delta\kappa^i\, \mathbf{D}^b\, \kappa^i\, dA = 0 \tag{3.11}$$

where $\delta\kappa^i$ denotes a virtual curvature field. It follows that at the solution point, κ^i vanishes pointwise provided the elastic coefficients matrix, $\mathbf{D}^b$, and all terms in equation $(3.9)_1$ are linearly independent. Similarly, taking the first variation of the energy functional with respect to γ^i shows that at the solution point, γ^i is zero pointwise. Consequently, the functions that satisfy the constraint equations form a subspace of the approximating spaces. Let these subspaces be denoted by a superscript "c" (e.g., $\mathbf{U}^c \subset \mathbf{U}^h$).

The elastic coefficients matrices $\mathbf{D}^b$ and $\mathbf{D}^s$ appearing in the constraint equation (3.10b), in general, vary over the element domain. As a result, imposing the constraint equation (3.10b) results in coupling the constant terms of the strain field with the nonconstant terms and consequently, failing the constant strain patch test. To avoid this problem, $\mathbf{D}^s$ and $\mathbf{D}^b$ are replaced by their mean values, denoted by a superposed bar, which are

defined as follows:

$$\bar{\mathbf{D}}^s := \frac{\int_A \mathbf{D}^s \, dA}{\int_A dA} \quad ; \quad \bar{\mathbf{D}}^b := \frac{\int_A \mathbf{D}^b \, dA}{\int_A dA} \tag{3.12}$$

Let the approximating fields, which satisfy the constraint equations (3.10), be given in each element by:

Box 3.2: Assumed Fields

• Moment field:	$\mathbf{M}^c := \tilde{\mathbf{M}}(\xi)\,\mathbf{m} + \mathbf{S}(\xi)\,\mathbf{q}$
• Transverse shear resultant field:	$\mathbf{Q}^c := \tilde{\mathbf{Q}}(\xi)\,\mathbf{q}$
• Curvature field:	$\kappa^c := \tilde{\kappa}(\xi)\,\mathbf{k} + \mathbf{R}(\xi)\,\mathbf{e}$
• Transverse shear strain field:	$\gamma^c := \tilde{\gamma}(\xi)\,\mathbf{e}$
• Displacement field:	$\mathbf{U} := \mathbf{N}(\xi)\,\mathbf{d}$

where $\mathbf{m}$, $\mathbf{q}$, $\mathbf{k}$, $\mathbf{e}$, and $\mathbf{d}$ are the vectors of independent moment, transverse shear resultant, curvature, transverse shear strain, and displacement parameters, respectively; $\tilde{\mathbf{M}}$, $\tilde{\mathbf{Q}}$, $\tilde{\kappa}$, and $\tilde{\gamma}$ are the matrices of shape functions for the moments, transverse shear resultants, curvatures, and transverse shear strain; in addition, $\mathbf{S}$ and $\mathbf{R}$ are the shape functions for the transverse shear strain coupling into the moment and curvature fields, respectively.

Remarks:

1. The coupling of the transverse shear resultant field into the moment field, and the coupling of the transverse shear strain field into the curvature field is the result of the constraint equations (3.10). Moreover, this form of coupling is consistent with the equilibrium equations, (2.7).
2. The shape functions are functions of the element natural coordinates $\xi^T = \left[\xi, \eta\right]$. ▪

In order to obtain a more compact form for the approximated Euler-Lagrange equations, the following definitions are introduced:

$$\begin{gathered}
\mathbf{H}^b_{kk} := \int_A \tilde{\kappa}^T \bar{\mathbf{D}}^b \, \tilde{\kappa} \, dA \quad ; \quad \mathbf{H}^b_{ke} := \int_A \tilde{\kappa}^T \bar{\mathbf{D}}^b \, \mathbf{R} \, dA \quad ; \\
\mathbf{H}^b_{ee} := \int_A \mathbf{R}^T \bar{\mathbf{D}}^b \, \mathbf{R} \, dA \quad ; \quad \mathbf{H}^s := \int_A \tilde{\gamma}^T \bar{\mathbf{D}}^s \, \tilde{\gamma} \, dA \quad ; \\
\mathbf{A}^s_{qe} := \int_A \tilde{\mathbf{Q}}^T \tilde{\gamma} \, dA \quad ; \quad \mathbf{A}^b_{mk} := \int_A \tilde{\mathbf{M}}^T \tilde{\kappa} \, dA \quad ; \quad \mathbf{A}^b_{me} := \int_A \tilde{\mathbf{M}}^T \mathbf{R} \, dA \quad ; \\
\mathbf{A}^b_{qk} := \int_A \mathbf{S}^T \tilde{\kappa} \, dA \quad ; \quad \mathbf{A}^b_{qe} := \int_A \mathbf{S}^T \mathbf{R} \, dA \quad ;
\end{gathered} \tag{3.13}$$

and

$$\mathbf{G}_m^b := \int_A \tilde{\mathbf{M}}^T \mathbf{B}^b \, dA \quad ; \quad \mathbf{G}_q^b := \int_A \mathbf{S}^T \mathbf{B}^b \, dA \quad ; \quad \mathbf{G}^s := \int_A \tilde{\mathbf{Q}}^T \mathbf{B}^s \, dA$$

In the above, $\mathbf{B}^b$ is the finite element curvature-displacement operator, defined by:

$$\mathbf{B}^b \, \mathbf{d} := \mathbf{L}^b \, \mathbf{U} \tag{3.14}$$

where $\mathbf{B}_I^b$ is associated with the node I and is given by:

$$\mathbf{B}_I^b := \begin{bmatrix} 0 & 0 & -N_{I,1} \\ 0 & N_{I,2} & 0 \\ 0 & N_{I,1} & N_{I,2} \end{bmatrix} \tag{3.15}$$

and $\mathbf{B}^s$ is the finite element shear strain-displacement operator, defined by:

$$\mathbf{B}^s \, \mathbf{d} := \mathbf{L}^s \, \mathbf{U} \tag{3.16}$$

where $\mathbf{B}_I^s$ is associated with the node I and is given by:

$$\mathbf{B}_I^s := \begin{bmatrix} N_{I,1} & 0 & N_I \\ N_{I,2} & -N_I & 0 \end{bmatrix} \tag{3.17}$$

Furthermore, let

$$\mathbf{H} := \begin{bmatrix} \mathbf{H}_{kk}^b & \mathbf{H}_{ke}^b \\ \mathbf{H}_{ke}^{bT} & \mathbf{H}_{ee}^e + \mathbf{H}^s \end{bmatrix} \; ; \; \mathbf{A} := \begin{bmatrix} \mathbf{A}_{mk}^b & \mathbf{A}_{me}^b \\ \mathbf{A}_{qk}^b & \mathbf{A}_{qe}^b + \mathbf{A}_{qe}^s \end{bmatrix} \; ; \tag{3.18}$$

and

$$\tau := \begin{bmatrix} \mathbf{m} \\ \mathbf{q} \end{bmatrix} \quad ; \quad \epsilon := \begin{bmatrix} \mathbf{k} \\ \mathbf{e} \end{bmatrix} \tag{3.19}$$

In the absence of "loading" terms from the constitutive equations (e.g., thermal loads), the Euler-Lagrange equations are approximated by:

$$\begin{bmatrix} \mathbf{H} & -\mathbf{A}^T & \mathbf{0} \\ -\mathbf{A} & \mathbf{0} & \mathbf{G} \\ \mathbf{0} & \mathbf{G}^T & \mathbf{0} \end{bmatrix} \begin{bmatrix} \epsilon \\ \tau \\ \mathbf{d} \end{bmatrix} = \begin{bmatrix} \mathbf{0} \\ \mathbf{0} \\ \mathbf{f} \end{bmatrix} \tag{3.20}$$

Elimination of the stress resultant coefficients, τ, and the strain coefficients, ϵ, from equation (3.19), for all elements yields:

$$\mathbf{K} \, \mathbf{d} = \mathbf{f}$$

where $\mathbf{K}$ is the finite element stiffness matrix, given by:

$$\mathbf{K} := \mathbf{G}^T \left(\mathbf{A} \, \mathbf{H}^{-1} \mathbf{A}^T \right)^{-1} \mathbf{G} \tag{3.21}$$

and $\mathbf{f}$ is the load vector, given by:

$$\mathbf{f} := \int_A \mathbf{N}\mathbf{F}\, dA + \int_{C_t} \mathbf{N}\mathbf{t}\, dA \tag{3.22}$$

If **A** is invertible, equation (3.21) can be replaced by:

$$\mathbf{K} := \mathbf{G}^T \mathbf{A}^{-T} \mathbf{H} \mathbf{A}^{-1} \mathbf{G} \tag{3.23}$$

which requires only one matrix inversion, and consequently is more computationally efficient. Moreover, since the strain and stress resultant interpolations are independent in each element, the reduction may be performed at the element level.

To satisfy stability conditions for every admissible displacement the following requirements must be satisfied (Zienkiewicz, *et al.* [1986]):

$$n_e + n_k + n_\theta \geq n_m \tag{3.24a}$$

$$n_e + n_k + n_\theta + n_w \geq n_q \tag{3.24b}$$

$$n_q \geq n_w \tag{3.24c}$$

$$n_m + n_q \geq n_\theta \tag{3.24d}$$

where n_e, n_k, n_m, n_q, n_θ, and n_w are the number of transverse shear, curvature, moment, transverse shear resultant, rotation, and transverse displacement independent parameters, respectively. Note, however, that to obtain the form given by equation (3.23), **A** must be a square matrix. This requirement is met if $n_e = n_q$ and $n_k = n_m$. Consequently, equations (3.24a,b) are identically satisfied.

The stress resultant and strain coefficients may be written in terms of the nodal displacement, **d**, as follows:

$$\mathbf{e} = \bar{\mathbf{A}}^{-1}[\mathbf{G}^s + \mathbf{G}_q^b - \mathbf{A}_{qk}^b (\mathbf{A}_{mk}^b)^{-1} \mathbf{G}_m^b]\mathbf{d} = F_1 \mathbf{d} \tag{3.25}$$

$$\mathbf{k} = (\mathbf{A}_{mk}^b)^{-1}[\mathbf{G}_m^b - \mathbf{A}_{me}^b F_1]\mathbf{d} = F_2 \mathbf{d} \tag{3.26}$$

$$\mathbf{q} = \bar{\mathbf{A}}^{-T}[(\mathbf{H}_{ke}^{bT} - \mathbf{H}_A) F_2 + (\mathbf{H}_{ee}^b + \mathbf{H}^s - \mathbf{H}_A) F_1]\mathbf{d} = F_3 \mathbf{d} \tag{3.27}$$

$$\mathbf{m} = (\mathbf{A}_{mk}^{bT})^{-1}[\mathbf{H}_{kk}^b F_2 + \mathbf{H}_{ke}^b F_1 - \mathbf{A}_{qk}^{bT} F_3]\mathbf{d} = F_4 \mathbf{d} \tag{3.28}$$

where

$$\bar{\mathbf{A}} := \mathbf{A}_{qe}^s - \mathbf{A}_{qk}^b (\mathbf{A}_{mk}^b)^{-1} \mathbf{A}_{me}^b + \mathbf{A}_{qe}^b \tag{3.29}$$

and

$$\mathbf{H}_A := \mathbf{A}_{me}^{bT} (\mathbf{A}_{mk}^b)^{-1} \mathbf{H}_{kk}^b \tag{3.30}$$

Remark: The Hu-Washizu-based procedure presented above can be reduced to a Hellinger-Reissner formulation by enforcing the stress-strain relation in a strong sense. It must be noted, however, that this reduction should be performed at the constraint equation

level. If it is performed at the functional level, the constraint equations are identically satisfied and thus, the desired structure cannot be obtained. ▪

The method presented above involves the use of incompatible displacements to generate the incompatible strains. A set of properties that these displacements must possess is presented in Weissman & Taylor [1990b], and is repeated in Box 3.3.

Box 3.3: Properties of the Incompatible Displacements

- Frame invariant,
- Do not bias the element in any direction,
- Simple functions (lowest order polynomial admissible),
- Higher order than the assumed compatible displacements (e.g., for the bilinear elements, at least quadratic),
- First derivatives vanish in a weak sense, and
- Preserve the sign convention used in the strong form (plates, shells, and beams).

For a discussion of these properties see Weissman & Taylor [1990b]. Attention should be drawn to the last requirement as it is crucial in the selection of incompatible functions for plate bending elements. This point will be demonstrated by numerical examples.

4. SHEAR LOCKING ANALYSIS

The major obstacle in the development of plate bending elements based upon theories that account for shear deformations is the well known locking behavior at the thin plate limit. In this section, it is proven that as a result of the couplings (transverse shear strain with curvature, and transverse shear with moment resultants) introduced in Section 3, shear locking is avoided at the element level.

Before proceeding with the proof, it is useful to give a precise definition of shear locking. To this end, note that for thin plates the displacements (i.e., rotations and transverse displacement) are $O(h^{-3})$. In addition, note that the moment and transverse shear resultants are determined by the equilibrium equations, and thus are $O(h^0)$. As the finite element methods are derived from energy principles, it is natural to define the numerical phenomenon of shear locking in terms of strain energy. In view of the above observations, and the constitutive relations, equations (2.8), shear locking is defined as

follows:

> Shear locking occurs in numerical approximation of thin plates if and only if the ratio of transverse shear strain energy to bending strain energy is $O(h^{\alpha})$, with $\alpha < 2$.

where $\alpha = 2$ is the result obtained by the Reissner-Mindlin theory at the thin plate limit, and $\alpha = -2$ for the four-node fully integrated isoparametric element which is known to exhibit severe locking when used to model thin plates.

First, it is assumed that the coupling introduced in the strain fields as well as that introduced in the stress resultant fields are fully ranked. It is proven, without resorting to the constraint count method, that shear locking at the thin plate limit is avoided. Second, the constraint on the rank of the coupling matrices is relaxed. It is shown that the results presented in the first part hold, provided the number of shear strain parameters not coupled into the curvature field and the number of shear resultant parameters not coupled into the moment field are both less than or equal to the number of constraints allowed per element by the constraint count method (see e.g., Hughes [1987]). In addition, in Proposition 4.5 it is shown that as the thickness is reduced to zero, convergence to the thin plate solution is obtained (also see remarks).

In order to simplify notations and without loss of generality, the plate thickness is assumed as constant over each elements' domain. In view of this assumption and the constraint equation (3.10b) the approximating transverse shear strain field is given by:

$$\gamma := h^2 \tilde{\gamma}\, \mathbf{e} \tag{4.1}$$

and consequently,

$$\mathbf{A}^s_{qe} := \int_A h^2 \tilde{\mathbf{Q}}^T \tilde{\gamma}\, dA \tag{4.2a}$$

and

$$\mathbf{H}^s := \int_A h^4 \tilde{\gamma}^T b D^s \tilde{\gamma}\, dA \tag{4.2b}$$

Proposition 4.1: Let the assumed strain and stress resultant fields be given by Box 3.2 with the transverse shear strain given by equation (4.1). Furthermore, let $\tilde{\mathbf{M}}$, $\mathbf{S}$, $\tilde{\mathbf{Q}}$, $\tilde{\kappa}$, $\mathbf{R}$, and $\tilde{\gamma}$ be of full rank. Then, as the thickness is reduced to zero, $\mathbf{F}_1$ and $\mathbf{F}_2$, defined by equations (3.24) and (3.25), respectively, are $O(h^0)$, while $\mathbf{F}_3$ and $\mathbf{F}_4$, defined by equations (3.26) and (3.27), respectively, are $O(h^3)$.

Proof: First note that $\mathbf{H}^b_{kk}$, $\mathbf{H}^b_{ke}$, and $\mathbf{H}^b_{ee}$ are $O(h^3)$; $\mathbf{H}^s$ is $O(h^5)$; $\mathbf{G}^b_m$, $\mathbf{G}^b_q$, and $\mathbf{G}^s$ are independent of h; $\mathbf{A}^b_{mk}$, $\mathbf{A}^b_{me}$, $\mathbf{A}^b_{qk}$, and $\mathbf{A}^b_{qe}$ are independent of h; and $\mathbf{A}^s_{qe}$ is $O(h^2)$. It follows that, as the thickness is reduced to zero, $\bar{\mathbf{A}}$, defined by equation (3.28), is given by:

$$\bar{\mathbf{A}} \approx \mathbf{A}^b_{qe} - \mathbf{A}^b_{qk} (\mathbf{A}^b_{mk})^{-1} \mathbf{A}^b_{me}$$

Consequently, the desired result follows. ▪

Proposition 4.2: Let the assumed stress resultant and strain fields be as in Proposition 4.1. If $\mathbf{F}_1$ and $\mathbf{F}_2$ are $O(h^0)$, and $\mathbf{F}_3$ and $\mathbf{F}_4$ are $O(h^3)$, then, as the element thickness is reduced to zero, the shear strain energy becomes negligible in comparison to the bending strain energy. Furthermore, the limit ratio of transverse shear strain energy to curvature strain energy is $O(h^2)$.

Proof: It follows from equation (3.31) that:

$$\mathbf{G}^b_q \mathbf{d} = \mathbf{A}^s_{qe} \mathbf{e} + \mathbf{A}^b_{qk} \mathbf{k} + \mathbf{A}^b_{qe} \mathbf{e} - \mathbf{G}^s \mathbf{d} \tag{4.4a}$$

$$\mathbf{A}^b_{mk} \mathbf{k} = \mathbf{G}^b_m \mathbf{d} - \mathbf{A}^b_{me} \mathbf{e} \tag{4.4b}$$

$$\mathbf{H}^b_{ke} \mathbf{e} = \mathbf{A}^{bT}_{mk} \mathbf{m} + \mathbf{A}^{bT}_{qk} \mathbf{q} - \mathbf{H}^b_{kk} \mathbf{k} \tag{4.4c}$$

and

$$\mathbf{H}^b_{ee} = \mathbf{A}^{sT}_{qe} \mathbf{q} + \mathbf{A}^{bT}_{me} + \mathbf{A}^{bT}_{qe} - \mathbf{H}^{bT}_{ke} \mathbf{k} - \mathbf{H}^s \mathbf{e} \tag{4.4d}$$

Substituting equations (4.4) into equation (3.27), and neglecting the external work, yields the following expression for the strain energy:

$$\Pi_{HW}(\mathbf{m}, \mathbf{q}, \mathbf{e}, \mathbf{k}, \mathbf{d}) = \frac{1}{2} [\mathbf{k}^T \mathbf{A}^{bT}_{mk} \mathbf{m} + \mathbf{k}^T \mathbf{A}^{bT}_{qk} \mathbf{q} + \mathbf{e}^T \mathbf{A}^{bT}_{me} \mathbf{m} + \mathbf{e}^T (\mathbf{A}^{bT}_{qe} + \mathbf{A}^{sT}_{qe}) \mathbf{q}] \tag{4.5}$$

It follows from the assumed order of $\mathbf{F}_1$, $\mathbf{F}_2$, $\mathbf{F}_3$, and $\mathbf{F}_4$ that the last term in equation (4.5), associated with the shear strain energy, is negligible in comparison to the first four terms, which are associated with the bending strain energy. Consequently, as the thickness is reduced to zero, the shear strain energy becomes negligible in comparison to the bending strain energy. Moreover, the desired ratio of $O(h^2)$ (at the thin plate limit) is obtained. ▪

Proposition 4.3: Shear locking is avoided if and only if the shear strain energy is negligible in comparison to the bending strain energy.

Proof: Assume the shear strain energy is negligible in comparison to the bending strain energy; it follows from the definition of shear locking that it does not occur.

Now assume that shear locking does not occur. $\mathbf{M}$ and $\mathbf{Q}$ are defined by equilibrium equations and are $O(h^0)$. Furthermore, $\mathbf{F}_4$ is $O(h^3)$ independent of the coupling. It follows that the elements of the vector $\mathbf{d}$ are $O(h^{-3})$. As a result, $\mathbf{e}$ and $\mathbf{k}$ are $O(h^{-3})$, and $\mathbf{m}$ and $\mathbf{q}$ are $O(h^0)$. It follows from equation (4.5) that the shear strain energy becomes negligible in comparison to the bending strain energy as the thickness is reduced to zero. ▪

So far it has been assumed that $\tilde{\mathbf{M}}$, $\mathbf{S}$, $\tilde{\mathbf{Q}}$, $b\tilde{K}a$, $\mathbf{R}$ and $\tilde{\gamma}$ are fully ranked. The question arises, what if $\mathbf{S}$ and $\mathbf{R}$ are not fully ranked? To answer this question, note that the

constraint is on the transverse shear strain. Consequently, only the rank deficiency of $\mathbf{R}$ is of importance, as long as the rank deficiency of $\mathbf{S}$ is less or equal to the rank deficiency of $\mathbf{R}$. This is shown below.

Proposition 4.4: $\bar{\mathbf{A}}$ is $O(h^0)$ independent of the coupling introduced between the assumed shear strain and assumed curvature.

Proof: In the case when $\mathbf{R}$ is rank deficient, the assumed shear strain is given by:

$$\gamma = h^2 \bar{\gamma}_1 \mathbf{e}_1 + \bar{\gamma}_2 \mathbf{e}_2 \tag{4.6}$$

where $\mathbf{e}_1$ are the shear strain coefficients coupled into the curvature, and $\mathbf{e}_2$ are the shear strain coefficients not coupled into the curvature. Consequently, the following structure is induced on $\mathbf{A}^s_{qe}$:

$$\mathbf{A}^s_{qe} = \begin{Bmatrix} h^2 \mathbf{A}^s_1 \\ \mathbf{A}^s_2 \end{Bmatrix}$$

The desired result follows. ∎

Remark: The above proof holds as long as the rank deficiency of $\mathbf{S}$ is less than or equal to the rank deficiency of $\mathbf{R}$. This may be seen directly from the structure of $\bar{\mathbf{A}}$. ∎

Let the shear coefficients $\mathbf{q}$ be given by:

$$\mathbf{q}^T = < \bar{\mathbf{q}}_1 , \bar{\mathbf{q}}_2 > \tag{4.7}$$

and let the displacement vector $\mathbf{d}$ be given by:

$$\mathbf{d} = \sum_{i=0}^{n} h^{i-3} \hat{\mathbf{d}}_i \tag{4.8}$$

where $\hat{\mathbf{d}}_i$ are independent of h.

Proposition 4.5: If the rank deficiency of $\mathbf{R}$ is less than or equal to the maximum number of constraints allowed per element by the constraint count method, and provided the rank deficiency of $\mathbf{S}$ is less than or equal to the rank deficiency of $\mathbf{R}$, then, $\bar{\mathbf{q}}_2$ is $O(h^0)$ and the shear strain, γ, is $O(h^{-1})$.

Proof: First note that by Proposition 4.4 $\bar{\mathbf{A}}$ is $O(h^0)$. Secondly, note that it follows from Proposition 4.4 that $\mathbf{F}_1$ and $\mathbf{F}_2$ are $O(h^0)$.

It follows from the structure of equation (3.26) that $\bar{\mathbf{q}}_1 = \bar{\mathbf{F}}_{31}\mathbf{d}$ and $\bar{\mathbf{q}}_2 = \bar{\mathbf{F}}_{32}\mathbf{d}$, where $\bar{\mathbf{F}}_{31}$ is $O(h^3)$, and $\bar{\mathbf{F}}_{32}$ is $O(h^1)$. As $\mathbf{d}$ is $O(h^{-3})$, and $\mathbf{Q}$ is determined by equilibrium and thus is $O(h^0)$, there is a contradiction. It follows that the contradiction is resolved if and only if $\bar{\mathbf{F}}_{32}$ is orthogonal to $\hat{\mathbf{d}}_0$ and $\hat{\mathbf{d}}_1$. Consequently, $\bar{\mathbf{q}}_2$ is $O(h^0)$.

The assumption on the number of constraints implies that shear locking does not occur. Consequently, by Proposition 4.3, the shear strain energy becomes negligible in comparison to the bending strain energy at the thin plate limit. Therefore, by equation (4.5) $\mathbf{e}_2$ must be $O(h^{\alpha})$ with $\alpha > -3$.

Let $\mathbf{e}_2 = \bar{\mathbf{F}}_{12}\mathbf{d}$ and $\mathbf{e}_1 = \bar{\mathbf{F}}_{11}\mathbf{d}$. Now, in order for $\bar{\mathbf{F}}_{32}$ to be orthogonal to $\hat{\mathbf{d}}_0$ and $\hat{\mathbf{d}}_1$, $\bar{\mathbf{F}}_{12}$ must be orthogonal to both $\hat{\mathbf{d}}_0$ and $\hat{\mathbf{d}}_1$. Consequently, taking notice of equation (4.6) and the fact that $\mathbf{F}_1$ is $O(h^{n0})$ results in the assumed shear strain $O(h^{-1})$. ▪

Remarks:

- It follows from Proposition 4.5 that the solution obtained by this formulation converges to the thin plate solution as the thickness is reduced to zero. It must be noted, however, that this convergence is obtained only when the solution of the plate theory used converges to the thin plate solution.
- If the couplings (introduced in Section 3) are neglected, the analysis predicts locking at the element level and consequently, analysis at the global level is required to determine whether shear locking occurs.

5. ELEMENT CONSTRUCTION

Four-node quadrilateral plate bending elements are used to illustrate the formulation presented in Section 3. The displacement, stress, and strain fields are given first. These are followed by the incompatible functions used.

5.1 Displacement Field

The standard isoparametric displacement field is given by:

$$\mathbf{U} = N_I\, d_I \tag{5.1}$$

where N_I is the shape function associated with node I, and d_I is the nodal displacement vector. The shape functions for four-node quadrilateral elements are given by:

$$N_I(\xi,\eta) = \frac{1}{4}(1+\xi_I\xi)(1+\eta_I\eta) \tag{5.2}$$

where ξ and η are the element natural coordinates, on the interval [-1,1], and ξ_I and η_I are the values of the natural coordinates at the node I.

It is commonly accepted that passing the constant strain patch test is an indication of good elements. Thus, plate bending elements are required to be able to represent exactly constant curvature and constant shear. The former is characterized by a state of biquadratic transverse displacements and bilinear rotation fields (no shear deformations), while

the latter is characterized by a state of bicubic transverse displacements and biquadratic rotation fields. Consequently, bilinear plate bending elements are bound to fail the constant strain patch test.

Remark: Parallelogram shaped elements do pass the constant strain patch test. This pathology is a manifestation of the mean-value theorem for integrals. ▪

Exact representation of constant curvature by arbitrary quadrilateral elements can be obtained if the approximation of the displacement field is slightly modified. To this end, note that a bilinear rotation field is the exact one for this case. In addition, note that the transverse shear is identically zero everywhere. Consequently, the Kirchoff assumption holds, and the rotation field can be used to enhance the displacement field (a similar approach was taken by Morris [1986], and implicitly by Bathe & Dvorkin [1985]).

The rotation field is assumed as a standard isoparametric field. Consequently, the assumed rotation field is given by:

$$\theta_\alpha = N_I \, \theta_{\alpha I} \tag{5.3}$$

where $\theta_{\alpha I}$ is the rotation θ_α at the node I.

It follows from the transverse shear strain displacement relation, equation (2.4a), that $w_{,\alpha} = -e_{\alpha\beta}\,\theta_\beta$. Thus, given the rotation field and the transverse displacement at a given point a, the transverse displacement at any point b can be computed as follows:

$$w_b = w_a + \int_a^b \theta_n(\xi,\eta)\, ds \tag{5.4}$$

where w_a and w_b are the transverse displacements at points a and b, respectively; and θ_n is the rotation about the normal to the line ab connecting points a and b. θ_n is given by:

$$\theta_n(\xi,\eta) = n_\alpha(\xi,\eta)\;\theta_\alpha(\xi,\eta) \tag{5.5}$$

where n_1 and n_2 are the components of the unit normal vector to the line ab.

Using the relations given by equations (5.4) and (5.5), the transverse displacements at the element mid-edge points can be computed as follows:

$$w_{i+4} = \frac{1}{2}\left(w_i + w_k + \int_i^{i+4} \theta_{ni}\, ds - \int_{i+4}^{k} \theta_{ni}\, ds\right) \tag{5.6}$$

where i=1,2,3,4; and k = (i+4) modulo 4. The "node" numbering and the normals to the paths used are presented in Figure 5.1. The transverse displacement at the element center ($\xi = \eta = 0$) can be computed as follows:

$$w_9 = \frac{1}{4}\sum_{i=5}^{8}\left(w_i + \int_i^9 \theta_{ni}\, ds\right) \tag{5.7}$$

The transverse displacement field can now be interpolated by

$$w(\xi,\eta) = \sum_{I=1}^{9} \bar{N}_I(\xi,\eta)\, w_I \tag{5.8}$$

where $\bar{N}_I$ are the standard quadratic nine-node Lagrangian element shape functions (see Zienkiewicz & Taylor [1989]).

Remarks:

- The consistent loading and consistent mass matrix must be modified to account for the enhanced interpolation used for the transverse displacement.
- When the simply supported boundary condition is specified as $w = M_n = M_{ns} = 0$ (the so called SS1 boundary condition), as a result of the enhanced interpolation used on the transverse displacement, the $w = 0$ condition is satisfied only at the nodes. w converges pointwise to zero, however, under mesh refinement.
- It must be emphasized that without the enhanced interpolation used for the transverse displacement, the proposed elements will not lock in shear (Weissman & Taylor [1990a]). The enhanced transverse displacement is introduced only in order to be able to represent a state of constant curvature/moment for elements distorted from a parallelogram shape.
- The general constant strain patch test requirement for plate bending elements necessitates the ability to exactly represent a state of constant shear strain/stress as well as that of constant curvature/moment. The scheme outlined above will not yield elements that can model a state of constant shear if the element is perturbed from a parallelogram shape. This remark, however, is true for all known four-node plate bending elements (e.g., T1 and Bathe & Dvorkin [1985] elements).
- It is common practice in the finite element literature to replace the constant shear strain patch test, as stated above, by a test in which the nodal rotations are constrained to be zero (i.e., shear deformation only). Indeed, the transverse displacement field for this case is bilinear. Consequently, all four-node elements can represent this case exactly. The plate bending elements presented in this work contain coupling between the shear strain and the curvature. Consequently, the curvature is not zero unless body couples are introduced. The shear strain, however, is exact. ▪

5.2 Moment Resultant Field

The assumed moment resultant field is taken as a complete linear field[2] in the element natural coordinates as follows:

[2] The stress resultant and strain fields are assumed as complete linear fields since this is the best assumption that may be used in conjunction with a bilinear displacement field.

$$\mathbf{M}^* = \begin{Bmatrix} M^*_{\xi\xi} \\ M^*_{\eta\eta} \\ M^*_{\xi\eta} \end{Bmatrix} = \begin{bmatrix} 1 & \xi & \eta & 0 & 0 & 0 & 0 & 0 & 0 \\ 0 & 0 & 0 & 1 & \xi & \eta & 0 & 0 & 0 \\ 0 & 0 & 0 & 0 & 0 & 0 & 1 & \xi & \eta \end{bmatrix} \begin{Bmatrix} m^*_1 \\ m^*_2 \\ \cdot \\ \cdot \\ m^*_9 \end{Bmatrix} \tag{5.9}$$

Since complete polynomials are used to express the membrane forces, equation (5.9) could be used for **M** directly. However, the reduction to satisfy the constraints introduced in Chapter 3 would require selection of different parameters in each element (i.e., there would be a dependence on element orientation of ξ and η with respect to x_1 and x_2). This dependence may be avoided by using the transformation procedure described below.

The following definitions are introduced:

$$xs = \frac{1}{4}\xi_I x_{1I} \;\; ; \;\; xt = \frac{1}{4}\eta_I x_{1I} \;\; ; \;\; xh = \frac{1}{4}(\xi\eta)_I x_{1I}$$

$$ys = \frac{1}{4}\xi_I x_{2I} \;\; ; \;\; yt = \frac{1}{4}\eta_I x_{2I} \;\; ; \;\; yh = \frac{1}{4}(\xi\eta)_I x_{2I}$$

Following Zienkiewicz & Taylor [1989], the Jacobian of the coordinate transformation from the (ξ, η) space to the (x_1, x_2) space is given by:

$$J = J_0 + J_1\xi + J_2\eta \tag{5.10}$$

where,

$$J_0 = xs \cdot yt - xt \cdot ys \quad ; \quad J_1 = xs \cdot yh - xh \cdot ys \quad ; \quad J_2 = xh \cdot yt - xt \cdot yh \tag{5.11}$$

The moment resultants in the physical space are obtained by using the following transformation:

$$M_{ij} = \frac{1}{J_0} F_{iI} F_{jJ} M^*_{IJ} \tag{5.12}$$

where both i and j take the values x_1 or x_2, and both I and J take the values ξ or η, and $F_{x,\xi} = \frac{\partial x_1}{\partial \xi}|_{\xi=\eta=0}$, etc. The transformation is based on values of **F** at the center of the element in order to maintain the constant terms decoupled from the nonconstant terms (Pian & Sumihara [1984]).

After redefining the independent coefficients, the assumed moment resultant field is given by:

$$\mathbf{M} = \begin{Bmatrix} M_{11} \\ M_{22} \\ M_{12} \end{Bmatrix} = \begin{bmatrix} 1 & 0 & 0 & xs^2\eta & xt^2\xi & xs^2\xi & xt^2\eta & 2xs\,xt\,\xi & 2xs\,xt\,\eta \\ 0 & 1 & 0 & ys^2\eta & yt^2\xi & ys^2\xi & yt^2\eta & 2ys\,yt\,\xi & 2ys\,yt\,\eta \\ 0 & 0 & 1 & xs\,ys\,\eta & xt\,yt\,\xi & xs\,ys\,\xi & xt\,yt\,\eta & A\,\xi & A\,\eta \end{bmatrix} \begin{Bmatrix} m_1 \\ m_2 \\ \cdot \\ \cdot \\ m_9 \end{Bmatrix} \tag{5.13}$$

where $A = xs \cdot yt + xt \cdot ys$.

With this construction, m_6, m_7, m_8, and m_9 may always be eliminated in satisfying equation (3.10a).

5.3 Transverse Shear Resultant Field

The transverse shear resultant field is constructed in a manner similar to that described above for the moment resultant field. Accordingly, let the assumed linear resultant field in the element natural space be given by:

$$\mathbf{Q}^* = \begin{Bmatrix} Q^*_\xi \\ Q^*_\eta \end{Bmatrix} = \begin{bmatrix} 1 & \xi & \eta & 0 & 0 & 0 \\ 0 & 0 & 0 & 1 & \xi & \eta \end{bmatrix} \begin{Bmatrix} q^*_1 \\ q^*_2 \\ \cdot \\ \cdot \\ q^*_6 \end{Bmatrix} \tag{5.14}$$

The shear resultant field in the physical space is obtained by means of the following transformation:

$$Q_i = \frac{1}{J_0} F_{iI} Q^*_I \tag{5.15}$$

where i takes the values x_1 or x_2, and I takes the values ξ or η. After redefining the independent shear coefficients, the assumed shear resultant field in the physical space is given by:

$$\mathbf{Q} = \begin{Bmatrix} Q_1 \\ Q_2 \end{Bmatrix} = \begin{bmatrix} 1 & 0 & xs\,\eta & xt\,\xi & xs\,\xi & xt\,\eta \\ 0 & 1 & ys\,\eta & yt\,\xi & ys\,\xi & yt\,\eta \end{bmatrix} \begin{Bmatrix} q_1 \\ q_2 \\ \cdot \\ \cdot \\ q_6 \end{Bmatrix} \tag{5.16}$$

With the above construction, the parameter set $\{q_5, q_6\}$ may always be selected as the set to be eliminated in satisfying equation (3.10a).

5.4 Curvature Field

The assumed curvature field is formulated in the element natural coordinates, and then transformed into the physical domain. Two types of transformations can be used:

- The same transformation as used for the moment resultant field.
- The inverse to the transformation used for the moment resultant field.

The first approach is motivated by the simplicity obtained when the same functions are used for both the moment and curvature fields. The second approach is motivated by the invariance of the complementary energy ($\sigma_{ij}\,\epsilon_{ij}$) under coordinate transformation. Accordingly, the transformation of a tensor of order two is given by:[3]

$$\mathbf{M}_{ij} = J\, F_{Ii}^{-1} F_{Jj}^{-1} \mathbf{M}_{IJ}^{*} \tag{5.17}$$

A similar approach was taken by Simo & Rifai [1989].

Following the path established in the assumed stress fields, the curvature field is assumed as a complete linear field in the element natural coordinates, and then transformed into the physical space. Using the transformation given by equation (5.12) yields:

$$\kappa = \begin{Bmatrix} \kappa_{11} \\ \kappa_{22} \\ \kappa_{12} \end{Bmatrix} = \begin{bmatrix} 1 & 0 & 0 & xs^2\eta & xt^2\xi & xs^2\xi & xt^2\eta & 2\,xs\,xt\,\xi & 2\,xs\,xt\,\eta \\ 0 & 1 & 0 & ys^2\eta & yt^2\xi & ys^2\xi & yt^2\eta & 2\,ys\,yt\,\xi & 2\,ys\,yt\,\eta \\ 0 & 0 & 1 & xs\,ys\,\eta & xt\,yt\,\xi & xs\,ys\,\xi & xt\,yt\,\eta & A\,\xi & A\,\eta \end{bmatrix} \begin{Bmatrix} k_1 \\ k_2 \\ \cdot \\ \cdot \\ k_9 \end{Bmatrix} \tag{5.18a}$$

and using the inverse transformation, equation (5.17), yields:

$$\kappa = \begin{bmatrix} 1 & 0 & 0 & yt^2\eta & xt^2\xi & yt^2\xi & xt^2\eta & -2\,yt\,xt\,\xi & -2\,yt\,xt\,\eta \\ 0 & 1 & 0 & ys^2\eta & xs^2\xi & ys^2\xi & xs^2\eta & -2\,ys\,xs\,\xi & -2\,ys\,xs\,\eta \\ 0 & 0 & 1 & -yt\,ys\,\eta & -xt\,xs\,\xi & -yt\,ys\,\xi & -xt\,xs\,\eta & A\,\xi & A\,\eta \end{bmatrix} \begin{Bmatrix} k_1 \\ k_2 \\ \cdot \\ \cdot \\ k_9 \end{Bmatrix} \tag{3.18b}$$

With the above construction, the parameter set $\{k_6, k_7, k_8, k_9\}$ may always be selected as the set to be eliminated in satisfying equation (3.10b).

5.5 Transverse Shear Strain Field

The transverse shear strain field is constructed in a manner similar to that described above for the curvature field. The (inverse) transformation is given by:

3 In direct notation, equation (6.23) would read: $\mathbf{M} = J\, F^{-1}\, \mathbf{M}^{*}\, F^{-T}$

$$\gamma_i = J F_{Ii}^{-1} \gamma_I^* \tag{5.19}$$

The assumed transverse shear strain in the physical space, using equation (5.15), is given by:

$$\gamma = \begin{Bmatrix} \gamma_1 \\ \gamma_2 \end{Bmatrix} = \begin{bmatrix} 1 & 0 & xs\,\eta & xt\,\xi & xs\,\xi & xt\,\eta \\ 0 & 1 & ys\,\eta & yt\,\xi & ys\,\xi & yt\,\eta \end{bmatrix} \begin{Bmatrix} e_1 \\ e_2 \\ \cdot \\ \cdot \\ e_6 \end{Bmatrix} \tag{5.20a}$$

and when using the inverse transformation, equation (5.19), the transverse shear strain field is given by:

$$\gamma = \begin{bmatrix} 1 & 0 & yt\,\eta & -xt\,\xi & yt\,\xi & -xt\,\eta \\ 0 & 1 & -ys\,\eta & xs\,\xi & -ys\,\xi & xs\,\eta \end{bmatrix} \begin{Bmatrix} e_1 \\ e_2 \\ \cdot \\ \cdot \\ e_6 \end{Bmatrix} \tag{5.20b}$$

With the above construction, the parameter set $\{e_5, e_6\}$ may always be selected as the set to be eliminated in satisfying equation (3.10b).

5.6 Incompatible Displacements

Let the assumed incompatible displacements be given by:

$$\theta_1^i = N_1^i \lambda_3 + N_2^i \lambda_4 \tag{5.21a}$$

$$\theta_2^i = N_1^i \lambda_5 + N_2^i \lambda_6 \tag{5.21b}$$

and

$$w^i = N_3^i \lambda_1 + N_4^i \lambda_2 \tag{5.21c}$$

where λ_1, λ_2, ..., and λ_6 are the independent incompatible displacement parameters, and $\mathbf{N}^i$ are the incompatible shape functions.

Remark: Different incompatible shape functions are used for the assumed incompatible transverse displacement since a higher order interpolation is used to model the transverse displacement (Section 5.1). ▪

To illustrate the motivation for the last requirement of the incompatible shape functions two options are used for N_1^i and N_2^i. The first set of functions (Wu, *et al.* [1987]) is given by:

$$N_1^i = \xi^2 - \frac{2J_1}{3J_0}\xi + \frac{2J_2}{3J_0}\eta \tag{5.22a}$$

$$N_2^i = \eta^2 + \frac{2J_1}{3J_0}\xi - \frac{2J_2}{3J_0}\eta \tag{5.22b}$$

The second set of functions (Taylor, *et al.* [1986]) is given by:

$$N_1^i = (1 - \frac{J_2}{J_0}\eta)(1-\xi^2) + \frac{J_1}{J_0}\xi(1-\eta^2) \tag{5.22a}$$

$$N_2^i = (1 - \frac{J_1}{J_0}\xi)(1-\eta^2) + \frac{J_2}{J_0}\eta(1-\xi^2) \tag{5.22b}$$

The second set satisfies all the requirements presented in Box 3.2, while the first set does not satisfy the last one. In addition, Note that the second set of incompatible modes is zero (compatible) at the nodal points while the first set is not.

The following functions are used for N_3^i and N_4^i the (Wu, *et al.* [1987]):

$$N_3^i = \xi^4 - \frac{4J_1}{5J_0}\xi + \frac{4J_2}{5J_0}\eta \tag{5.23a}$$

$$N_4^i = \eta^4 + \frac{4J_1}{5J_2}\xi - \frac{4J_2}{5J_0}\eta \tag{5.23b}$$

Remark: A study of the constraint equations (3.10) in component form shows that the last requirement in Box 3.2 does not apply to N_3^i and N_4^i. ▪

5.7 Proposed Elements

Six four-node quadrilateral plate bending elements are proposed. Two are formulated via the Hellinger-Reissner variational principle, and four via the Hu-Washizu variational principle. The class of elements developed here is labeled Coupled Resultants Bending (CRB).

The proposed elements are summarized in Table 6.1.

Table 6.1c Proposed Plate Bending Elements

Element	Formulation	Incompatible shape function equations	Strain transformation equations
CRB1	Hellinger-Reissner	(5.21)	-
CRB2	Hellinger-Reissner	(5.22)	-
CRB3	Hu-Washizu	(5.21)	(5.12) and (5.15)
CRB4	Hu-Washizu	(5.22)	(5.12) and (5.15)
CRB5	Hu-Washizu	(5.21)	(5.17) and (5.19)
CRB6	Hu-Washizu	(5.22)	(5.17) and (5.19)

6. NUMERICAL EXAMPLES

The performance of the plate bending (CRB) elements proposed in Chapter 5 are evaluated with several discriminating problems selected from the literature. Convergence of the results obtained by the four-node elements presented in Chapter 5 are compared with the S1 (Hughes, *et al.* [1978]) and T1 (Hughes & Tezduyar [1981]).

Three types of boundary conditions are used:

SS1 - Simply Supported, $w = M_n = M_{nt} = 0$.

SS2 - Simply Supported, $w = M_n = \theta_t = 0$.

CL - Clamped, $w = \theta_n = \theta_t = 0$.

In all examples identical results are obtained for elements formulated via the Hellinger-Reissner variational principle and the corresponding (i.e., same incompatible shape functions) elements formulated via the Hu-Washizu variational principle. Identical results are also obtained for the two approaches taken to transform the assumed strain field from the element's natural space into the physical space.

6.1 Patch Test

A rectangular domain is modeled by a single element as shown in Figure 6.1a and the skewed mesh as shown in Figure 6.1b. The mesh is subjected to constant states of bending, transverse shear and in-plane twist. All elements presented pass all tests with the exception of the constant transverse shear, when the skewed mesh is used. The failure of these elements to pass the constant shear patch test is discussed in detail in Section 5.2. Constant shear strain is modeled exactly, however, when all rotational degrees-of-freedom are fixed (this is the common test for constant shear in the finite element literature).

6.2 Beam Problems

These problems were suggested by MacNeal & Harder [1985] as standard problems to evaluate the performance of different elements. The meshes used contain only one row of six elements for both the straight beams, shown in Figure 6.2, and the curved beam, shown in Figure 6.3. Geometrical and material properties used are summarized in Table 6.1. Results are normalized with respect to solutions obtained by beam theory which are summarized in Table 6.2.

Table 6.1 Material and Geometrical Properties for Beam Problems						
	E	ν	thickness	length/ inner radius	width/ outer radius	arc
straight beam	1.0E+7	0.3	0.1	6.0	0.2	-
curved beam	1.0E+7	0.25	0.1	4.12	4.32	90^o

Table 6.2 Theoretical Solutions for Beam Problems		
Tip load direction	Displacement in the direction of the load	
	Straight beam	Curved beam
Out-of-plane shear	0.4321	0.5022
Twist	0.03208	-

6.2.1 Out-of-plane shear

Both the straight beams, Figure 6.2, and curved beam, Figure 6.3, meshes are used. The results, normalized by beam theory solution (see Table 6.2) are given in Table 6.3.

Table 6.3 Out-of-plane shear				
mesh	CRB1,3,5	CRB2,4,6	S1	T1
straight (a)	0.9825	0.9877	0.9801	0.9801
straight (b)	0.9706	0.9684	0.9963	0.9634
straight (c)	0.9843	0.9889	0.9912	0.9780
curved	0.9308	0.9248	29.535	0.9290

Very small sensitivity to the incompatible shape functions used is observed, less than 0.5% for all meshes. The CRB and T1 elements yield comparable results. The S1 element exhibits unstable behavior unstable behavior in the curved beam problem.

6.2.2 Twist of a beam

The straight beam meshes shown in Figure 6.2 are used. The results are normalized with the theoretical beam solution given in Table 6.2, and are summarized in Table 6.4.

Table 6.4 Twist of a straight beam				
mesh	CRB1,3,5	CRB2,4,6	S1	T1
straight (a)	0.9429	0.9373	377.36	0.9445
straight (b)	0.9882	0.9622	108.83	0.8844
straight (c)	0.9478	0.9412	138.16	0.8490

The S1 element shows instability in this problem. The proposed elements exhibit very small sensitivity to the incompatible shape functions used (maximum of 2.6% for mesh b).

6.3 Circular Plates

A circular plate is modeled using 3, 12, 48 and 192 elements. Due to symmetry, only one quadrant is discretized. A typical mesh used is shown in Figure 6.4. SS1 and CL boundary conditions are used. The material properties and geometrical data used are summarized in Table 6.5.

Table 6.5 Material and Geometrical Data for Circular plates

	E	ν	h	R
Thin Plate	10920	0.3	0.1	5.0
Thick Plate	1.365	0.3	2.0	5.0

With these properties the plate stiffness $D = \frac{E h^3}{12(1-\nu^2)} = 1.0$.

The plates are loaded by a uniform distributed transverse load. In addition, the case of a thick plate loaded by a unit point load at the center is considered in order to exhibit the stability of the proposed elements.

The analytical solution for the center transverse displacement and external work are given in Weissman & Taylor [1990a]. The energy expressions reported are for the total work performed by the external loads, and consequently are twice the actual strain energy.

6.3.1 Simply supported thin plate: Uniform transverse load

The analytical solutions are: w(0) = 39.83156 and E_{SS} = 359.08748. The results obtained, normalized with respect to these solutions, are shown in Figures 6.5 and 6.6 for the convergence of the center displacement and energy norm, respectively.

Monotonic convergence in both the energy norm and center transverse displacement is obtained for all elements. The proposed elements show some sensitivity to the type of incompatible shape functions used for coarse meshes, from 10.5% difference in the energy norm for the three-element mesh to only 1.5% difference for the 48-element mesh.

6.3.2 Clamped thin plate: Uniform transverse load

The analytical solutions are: w(0) = 9.78348 and E_{CL} = 64.09118. The results obtained, normalized with respect to these solutions, are shown in Figures 6.7 and 6.8 for the convergence of the center displacement and energy norm, respectively.

Monotonic convergence in both the energy norm and center transverse displacement is obtained for all elements. The proposed elements show great sensitivity to the type of incompatible shape functions used. 64% difference in the energy norm is observed for the three-element mesh. However, for the 192-element mesh, only 2.4% difference is observed

in the energy norm.

6.3.3 Clamped plates: Unit concentrated load at the center

The thick plate case is used to demonstrate the stability of the proposed elements. The transverse displacement along the radius, normalized with $\frac{P R^2}{16 \pi D}$, for a mesh of 48 elements, is shown in Figure 6.9. The analytical solution can be found in Lukasiewicz [1979]. The S1 shows the well known instability (Hughes [1987]); the T1 and all CRB elements, on the other hand, show excellent results.

6.4 Square Plates

A square plate is modeled using meshes of uniform square elements. Due to symmetry, only one quadrant is discretized. A typical mesh is shown in Figure 6.10. The material properties are: $E = 10.92E+6$ and $\nu = 0.3$, and the geometrical data is: $h = 0.01$ and $L = 10$. Using these properties, the plate bending stiffness D = 1.0.

Only the case of uniform transverse loading is examined. The boundary conditions examined are: SS1, SS2, and CL.

The "exact" energy reported is computed from:

$$E = \int_{\Omega} q(x_1,x_2)\, w(x_1,x_2)\, d\Omega \tag{4.1}$$

using a Fourier series solution and, thus, is twice the actual strain energy.

6.4.1 Thin simply supported (SS1) plate

The exact solution is $w = 40.623$ (Timoshenko & Woinowsky-Krieger [1959]) and $E = 425.6276$. Results, normalized with the exact solution, are shown in Figures 6.11 (center displacement) and 6.12 (energy).

With the exception of the one-element mesh, only mild sensitivity to the incompatible shape function used is observed. A difference of only 2.4% and 3.4% is observed in the center transverse displacement and energy norm, respectively, for the four-element mesh.

6.4.2 Thin simply supported (SS2) plate

The exact solution is $w = 40.623$ and $E = 425.6276$ (thick plate theory, series solution). Results, normalized with the exact solution, are shown in Figures 6.13 (center displacement) and 6.13 (energy).

As observed for the SS1 boundary condition, with the exception of the one-element mesh, only mild sensitivity to the incompatible shape function used is observed.

6.4.3 Thin clamped plate

The exact thin plate solution is $w = 12.6$ (Timoshenko & Woinowsky-Krieger [1959]). No analytical solution is available for the energy. Consequently, a converged finite element solution obtained using 4096 elements is used, $E = 97.3$. Results, normalized with these values, are shown in Figures 6.15 (center displacement) and 6.16 (energy).

The converged finite element solution of the transverse displacement is about 0.4% larger than the solution obtained by the thin plate theory. This result is expected since all the elements under discussion are based on a theory that accounts for shear deformation.

The S1 and T1 elements yield identical results. Both elements obtain monotonic convergence in both criteria. The CRB elements, on the other hand, do not converge monotonically. A small sensitivity to the incompatible shape functions is observed. Only about 1.5% difference is observed in both the energy norm and center transverse displacement for the 16-element mesh.

All elements exhibit locking for the one-element mesh. This result is expected since all rotational degrees-of-freedom are constrained, and consequently the rotations are zero pointwise in the element's domain. It follows from the shear strain transverse displacement relation (see Section 2) that the derivatives of the transverse displacement go to zero pointwise as the thickness is reduced to zero; consequently, the transverse displacement tends to zero as the plate thickness is reduced to zero.

6.4.4 Mesh distortion

To study the sensitivity to mesh distortion, a coarse mesh modeling a clamped square plate is used. Only four elements are used to model one quadrant of the plate. The plate is loaded by a uniform unit transverse load. Two types of distortion are introduced. First, the center node of the mesh is moved along the main diagonal of the plate as shown in Figure 6.17. Results, normalized with respect to the thin plate solution $w = 12.6$ (Timoshenko & Woinowsky-Krieger [1959]), are shown in Figure 6.18.

Next the center node is moved parallel to the edge as shown in Figure 6.19. Results, normalized with respect to the thin plate solution $w = 12.6$ are shown in Figure 6.20.

The difficulty of this mesh is that there are only eight degrees-of-freedom. The "optimal" number of constraints per element, according to the constraint count method, is two. Consequently, the ratio of degrees-of-freedom to constraints, for this mesh, is one.

Thus, shear locking becomes an important issue as the symmetry of the mesh is lost.

The proposed elements' performance deteriorates to about 66% of the solution. The T1 and S1 elements, on the other hand, exhibit severe locking.

6.4.5 Shear and moment resultants

These examples were proposed by Hinton & Huang [1986] as a set of tests designed to test the stress resultants recovered by the finite element approximation. A square plate, with SS1/SS2 boundary conditions and of side length $L = 10$, is modeled by a graded mesh as shown in Figure 6.21. Due to symmetry only one quadrant is discretized. The stress distributions inside the elements are reported. Results are compared to the solutions given by Kant & Hinton [1983].

The distribution of Q_1 along the line $x_2 = L/2$, and of Q_2 along the line $x_2 = 0$, for all CRB elements, are shown in Figures 6.22 and 6.23, respectively. The M_{12} distribution along the line $x_2 = 0$ is shown in Figure 6.24 for the CRB1,3,5 elements and in Figure 6.25 for the CRB2,4,6 elements.

The moment distribution inside the CRB1,3,5 elements has an opposing gradient to the exact moment gradient, which results from the fact that the incompatible shape functions do not satisfy the last requirement set in Box 3.3. On the other hand, the gradient inside the CRB2,4,6 elements has the correct orientation (incompatible shape functions satisfy all requirements set in Box 3.3). The transverse shear resultants are almost identical for all elements.

6.5 Rhombic Plates

In this standard test, a highly skewed rhombic plate of side length $L = 100.0$ and an acute angle $\Theta = 30^o$ is modeled by a uniform mesh. A typical mesh is shown in Figure 6.26. The material properties used are: $E = 10E+6$, $\nu = 0.3$ and $h = 1$. A comparison solution for the center displacement of $w = 0.04455$ was obtained by Morley [1963]. No solution is available, however, for the energy. Consequently, a converged finite element solution of $E = 78.9$ is used as a reference solution. Results normalized with the reference solution are shown in Figures 6.27 (center displacement) and 6.28 (energy). The distributions of M_{11} and M_{22} along the short diagonal are shown in Figures 6.29 (CRB1,3,5 elements) and 6.30 (CRB2,4,6 elements).

The converged center displacement is about 4% higher than the solution predicted by the thin plate theory (Morley [1963]). These results are in agreement with the observation made by Babuska and Scopolla [1989]. Results obtained by the proposed elements are

sensitive to the incompatible shape functions used for coarse meshes; 78% and 22% differences in the energy norm are observed for the four- and 16-element meshes, respectively.

As observed for the square plate, the moment slope orientation in the CRB1,3,5 elements is opposite to the slope orientation of the exact solution. The slope orientation in the CRB2,4,6 elements, on the other hand, is of the same orientation as the slope of the exact solution. It must be noted that the corner element exhibits a pathological behavior. Excellent behavior, however, is observed in all other elements. Moreover, note that good moments are recovered at the center of the corner element.

7. CONCLUDING REMARKS

The main objective of this paper is to present a formulation for plate bending finite elements, based on the Reissner-Mindlin theory, which leads to elements that avoid shear locking (at the thin plate limit) at the element level. The proposed formulation is derived via the Hu-Washizu functional. The Hellinger-Reissner formulation is also considered as a special case of the Hu-Washizu functional.

It is proven that the proposed formulation leads to elements free of locking. The proposed elements exhibit excellent results when subjected to an extensive numerical evaluation. In addition, good stress resultants are recovered at the element level.

Identical results are obtained for elements formulated via the Hellinger-Reissner and Hu-Washizu functionals, provided the same incompatible functions are used. Also, identical results are obtained for both approaches taken to transform the assumed strain field from the element's natural space into the physical space. However, the results are sensitive to the incompatible shape functions for coarse meshes.

REFERENCES

Babuska, I. & T. Scapolla, [1989], "Benchmark Computation and Performance Evaluation for a Rhombic Plate Bending Problem," *International Journal for Computer-Aided Engineering and Software*, Vol. 27, pp. 155-179.

Bathe, K.J. & E.N. Dvorkin, [1985], "A Four Node Plate Bending Element Based on Mindlin/Reissner Plate Theory and Mixed Interpolation," *International Journal for Numerical Methods in Engineering*, Vol. 18, pp. 1077-1089.

Fraeijs de Veubeke, B., [1965], "Displacement and Equilibrium Models in the Finite Element Method," in *Stress Analysis*, editors O.C. Zienkiewicz & G.S. Holister. London: John Wiley.

Hinton, E. & H.C. Huang, [1986], "Shear Forces and Twisting Moments in Plates Using Mindlin Elements," *Engineering Computations*, Vol. 3, pp. 129-142.

Hughes, T.J.R, M. Cohen & M. Haroun, [1978], "Reduced and Selective Integration Techniques in the Finite Element Analysis of Plates," *Nuclear Engineering and Design*, Vol. 46, pp. 203-222.

Hughes, T.J.R., [1987], *The Finite Element Method*, Prentice-Hall, Inc., Englewood Cliffs, New Jersey.

Hughes, T.J.R. & T.E. Tezduyar, [1981], "Finite Elements Based Upon Mindlin Plate Theory with Particular Reference to the Four Node Bilinear Isoparametric Element," *Journal of Applied Mechanics*, Vol. 46, pp. 587-596.

Kant, T. & E. Hinton, [1983], "Mindlin Plate Analysis by Segmentation Method," *Journal of Engineering Mechanics Division, ASCE*, Vol. 109, pp. 537-556.

Lukasiewicz, S., [1979], *"Local Loads in Plates and Shells,"* Sijthoff & Noordhoff, the Netherlands.

MacNeal, R.H. & R.L. Harder, [1985], "A Proposed Standard Set of Problems to Test Finite Element Accuracy," *Finite Elements in Analysis and Design*, Vol. 1, pp. 3-20.

Mindlin, R.D., [1951], "Influence of Rotatory Inertia and Shear in Flexural Motions of Isotropic Elastic Plates," *Journal of Applied Mechanics*, Vol. 18, pp. 31-38.

Morley, L.S.D., [1963], *Skew Plates and Structures*, International Series of Monographs in Aeronautics and Astronautics, New York.

Morris, G.R., [1986], "Kinematic Formulation of Finite Elements for Plate Bending," Ph.D. dissertation, University of California at Berkeley.

Pian, T.H.H. & K. Sumihara, [1984], "Rational Approach for Assumed Stress Finite Elements," *International Journal for Numerical Methods in Engineering*, Vol. 20, pp. 1685-1695.

Reissner, E., [1945], "The Effect of Transverse Shear Deformation on the Bending of Elastic Plates," *Journal of Applied Mechanics*, Vol. 12, pp. 69-76.

Simo, J.C. & M.S. Rifai, [1989], "A Class of Mixed Assumed Strain Methods and the Method of Incompatible Modes," to appear.

Taylor R.L., O.C. Zienkiewicz, J.C. Simo & A.H.C. Chan, [1986], "The Patch Test for Mixed Formulations," *International Journal for Numerical Methods in Engineering*, Vol. 22, pp. 32-62.

Timoshenko, S. & S. Woinowsky-Krieger, [1959], *Theory of Plates and Shells*, McGraw-Hill, New York.

Washizu, K. *Variational Methods in Elasticity and Plasticity*, Pergamon Press, Oxford, 1948.

Weissman, S.L. & R.L. Taylor, [1990a], "Resultant Fields for Mixed Plate Bending Elements," *Computer Methods in Applied Mechanics and Engineering*, Vol. 79, pp. 321-355.

Weissman, S.L. & R.L. Taylor, [1990b], "Treatment of Internal Constraints by Mixed Finite Element Methods: Unification of Concepts," Report No. UCB/SEMM-90/05.

Wu, C.-C., M.-G. Huang & T.H.H. Pian, [1987], "Consistency Condition and Convergence Criteria of Incompatible Elements: General Formulation of Incompatible Functions and its Application," *Computers & Structures*, Vol. 27, No. 5, pp. 639-644.

Zienkiewicz, O.C., S. Qu, R.L. Taylor & S. Nakazawa, [1986], "The Patch Test for Mixed Formulations," *International Journal for Numerical Methods in Engineering*, Vol. 23, pp. 1873-1883.

Zienkiewicz, O.C. & R.L. Taylor, [1989], *The Finite Element Method*, 4th edition, MacGraw-Hill Book Co., London.

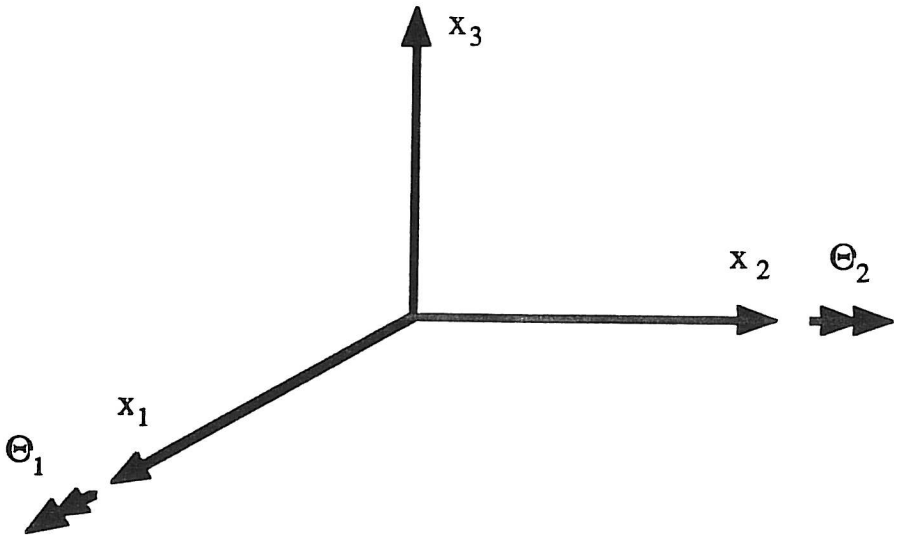

Figure 2.1: Sign convention for rotations, right-hand-rule rotations.

$$\gamma_\alpha = W_{,\alpha} + e_{\alpha\beta}\,\Theta_\beta$$

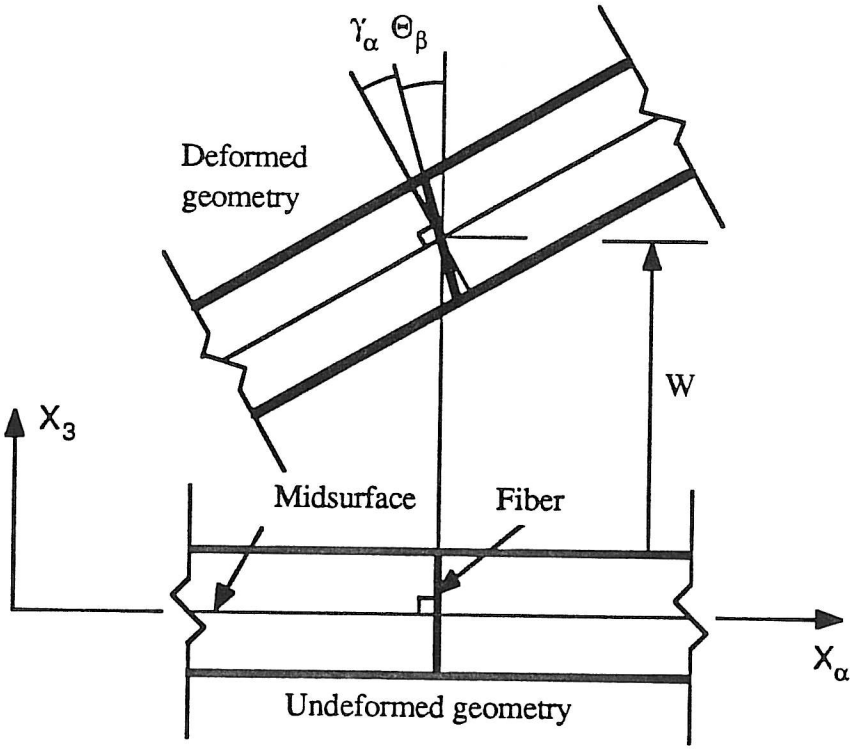

Figure 2.2: Plate kinematics.

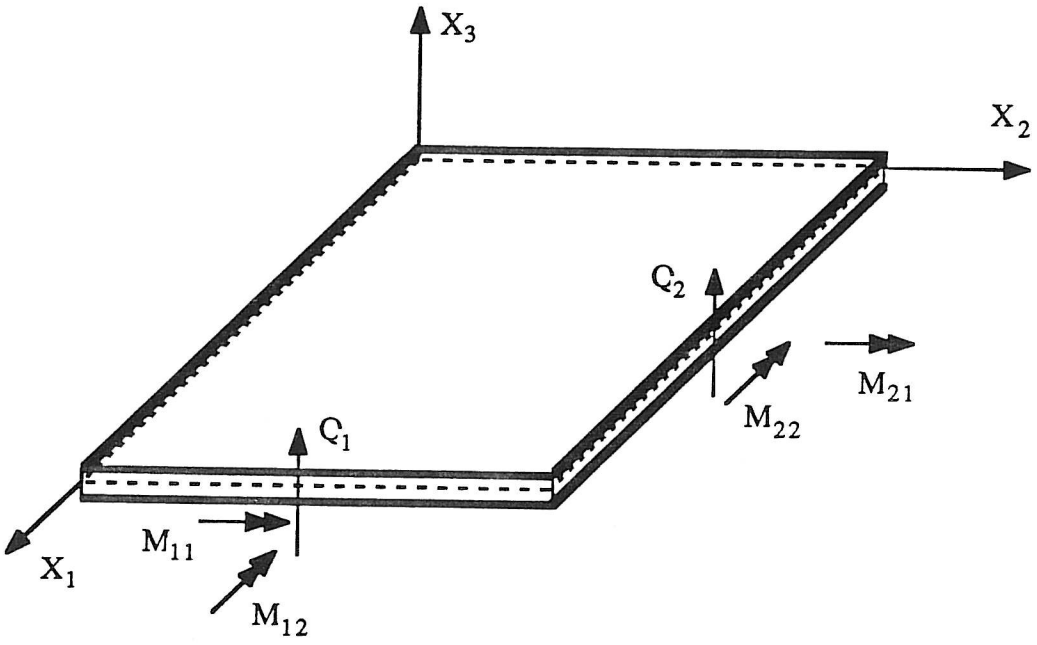

Figure 2.3: Sign convention for stress resultants on positive faces.

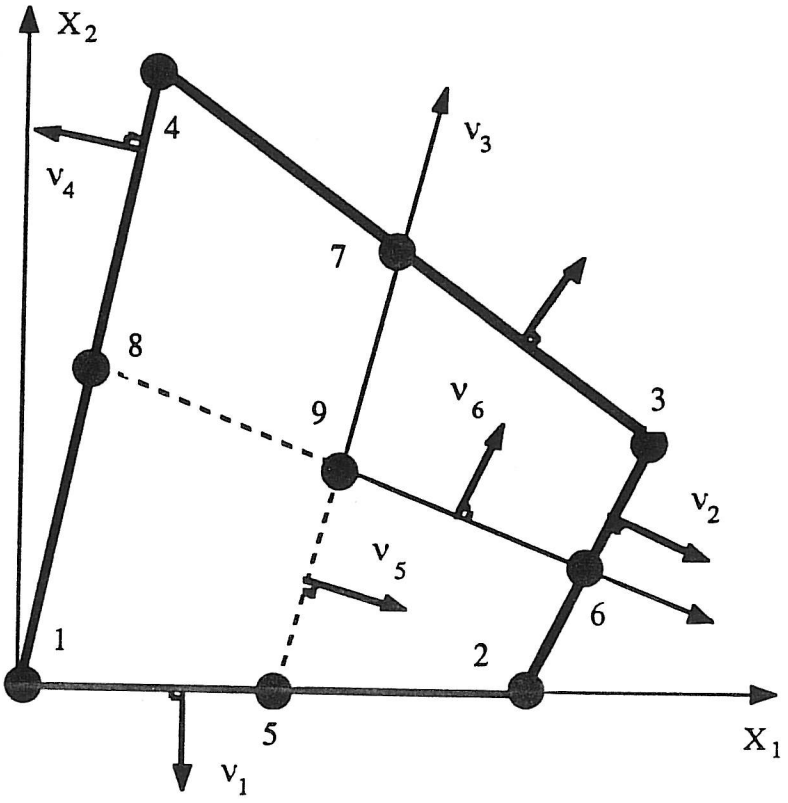

Figure 5.1: Location of the additional five "nodes" (numbers 5-9) and the normals to the paths used in the integration scheme to provide enhanced interpolation for the transverse displacement.

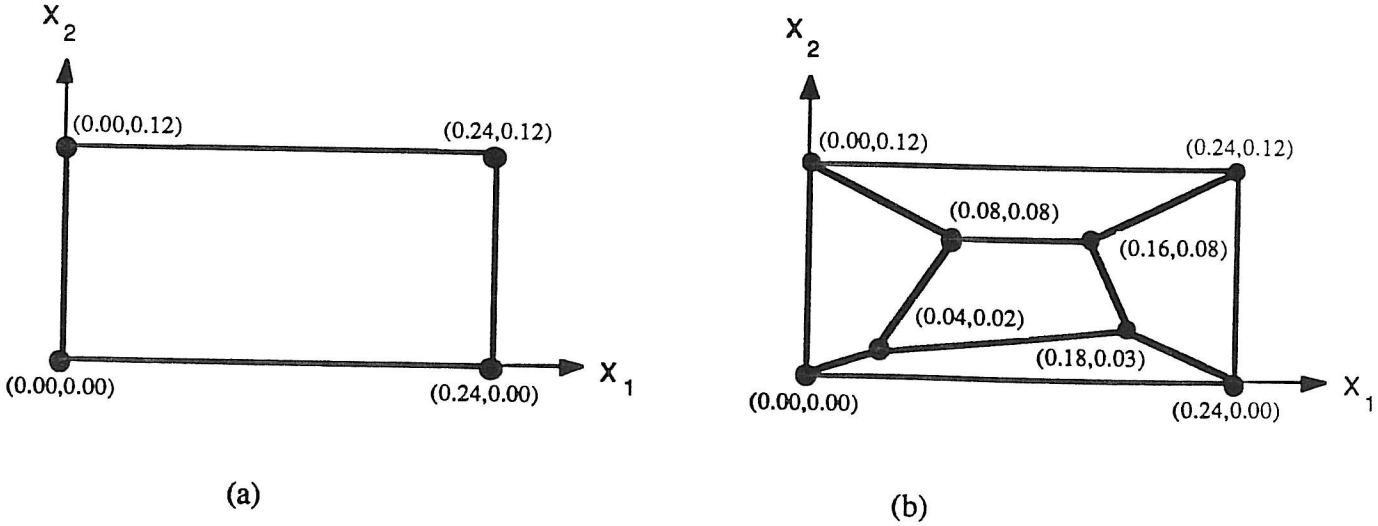

Figure 6.1: Patch test - (a) One-element mesh, (b) Skewed mesh.

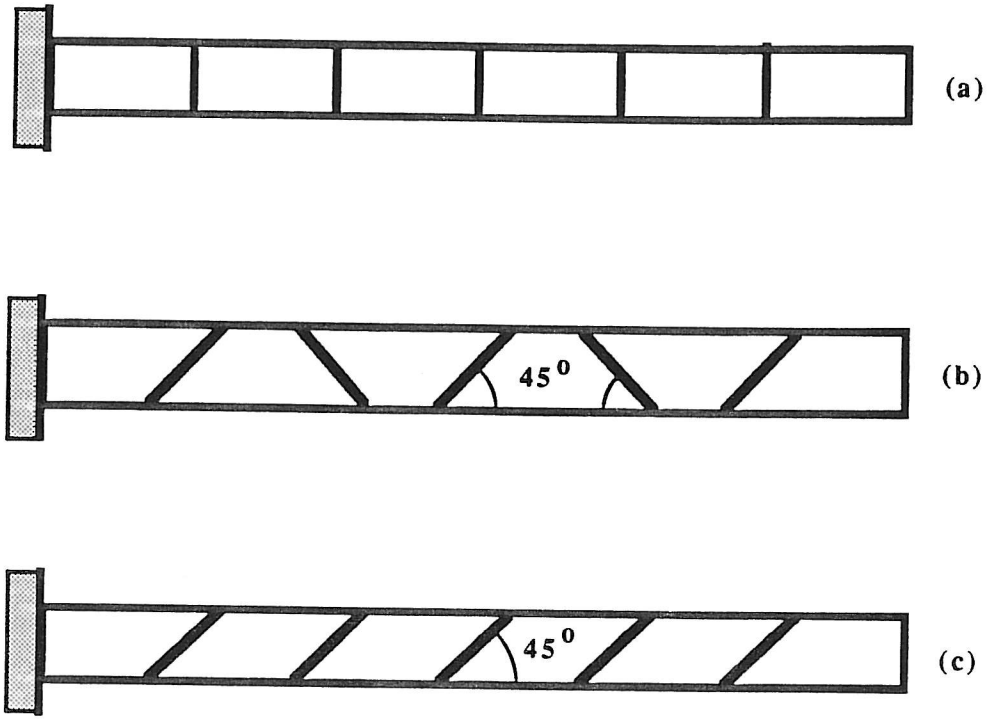

Figure 6.2: Straight cantilever beam. (a) Regular shape elements; (b) Trapezoid shape elements; (c) Parallelogram shape elements.

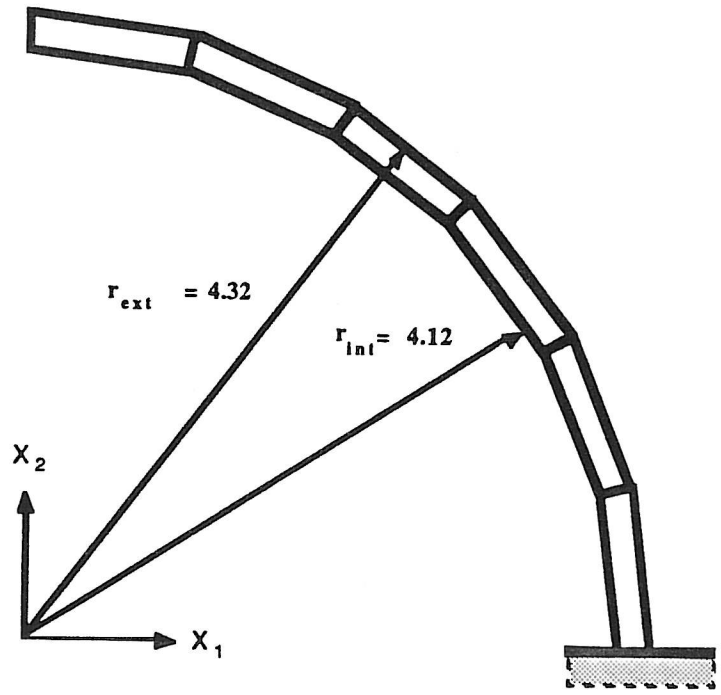

Figure 6.3: Curved beam mesh.

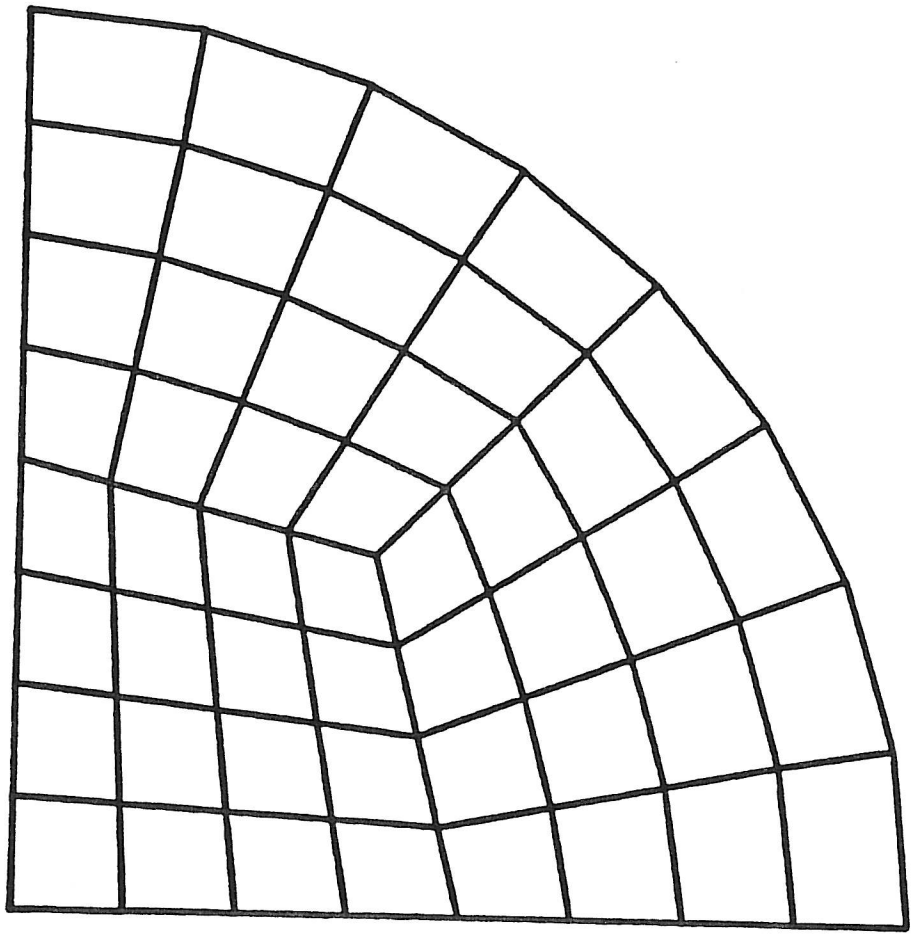

Figure 6.4: Circular plate. Due to symmetry only one quadrant is discretized.

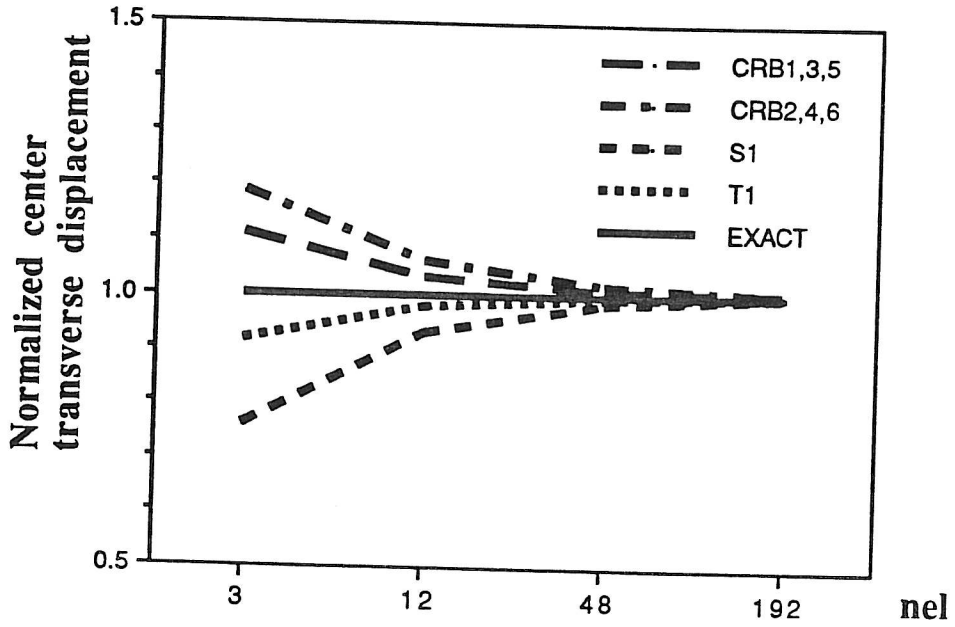

Figure 6.5: Simply supported (SS1) thin circular plate; uniform load; convergence of center transverse displacement.

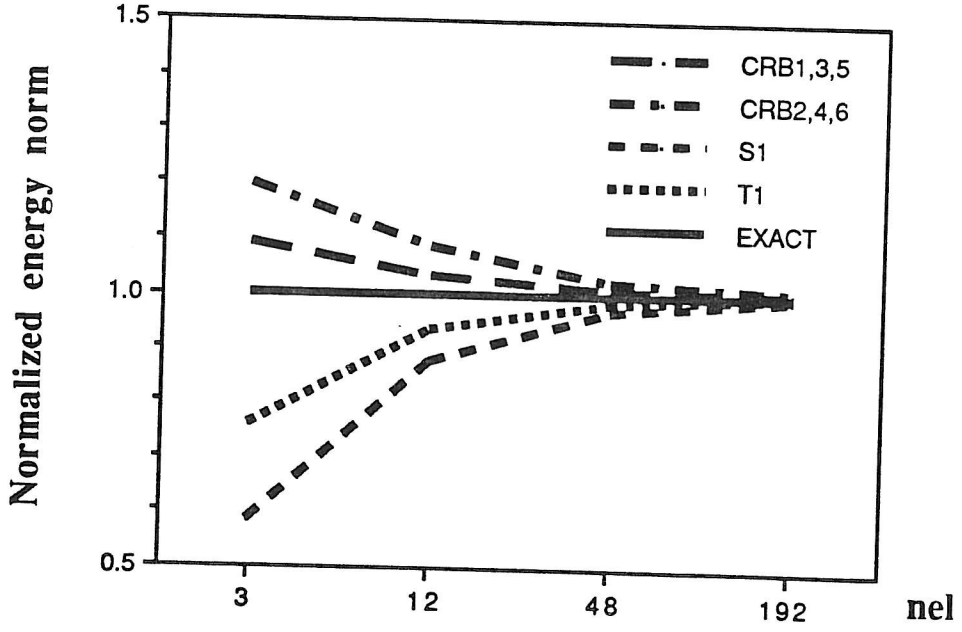

Figure 6.6: Simply supported (SS1) thin circular plate; uniform load; convergence in the energy norm.

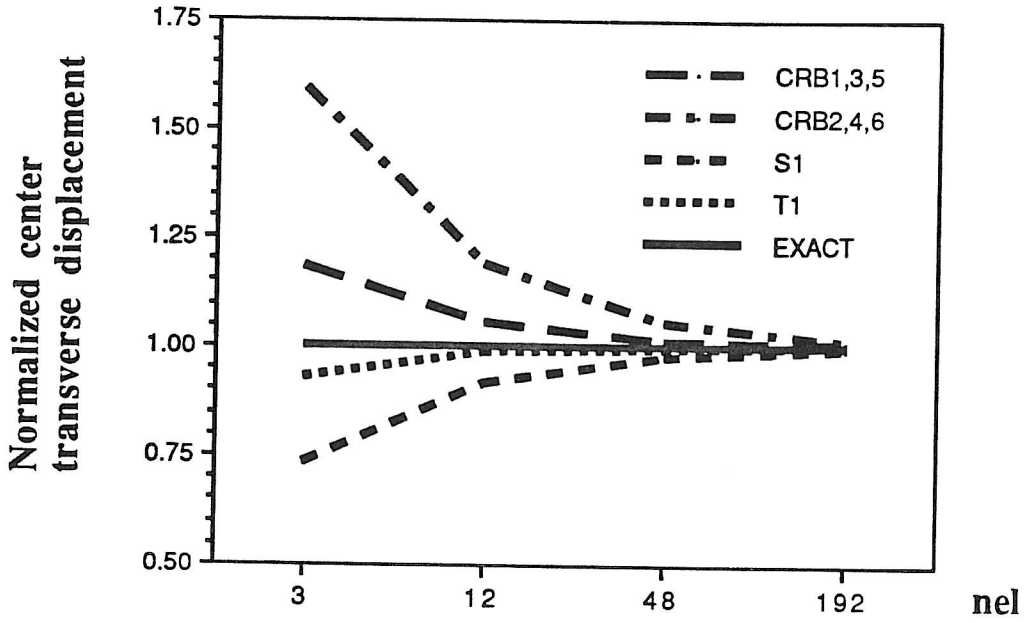

Figure 6.7: Clamped thin circular plate; uniform load; convergence of the center transverse displacement.

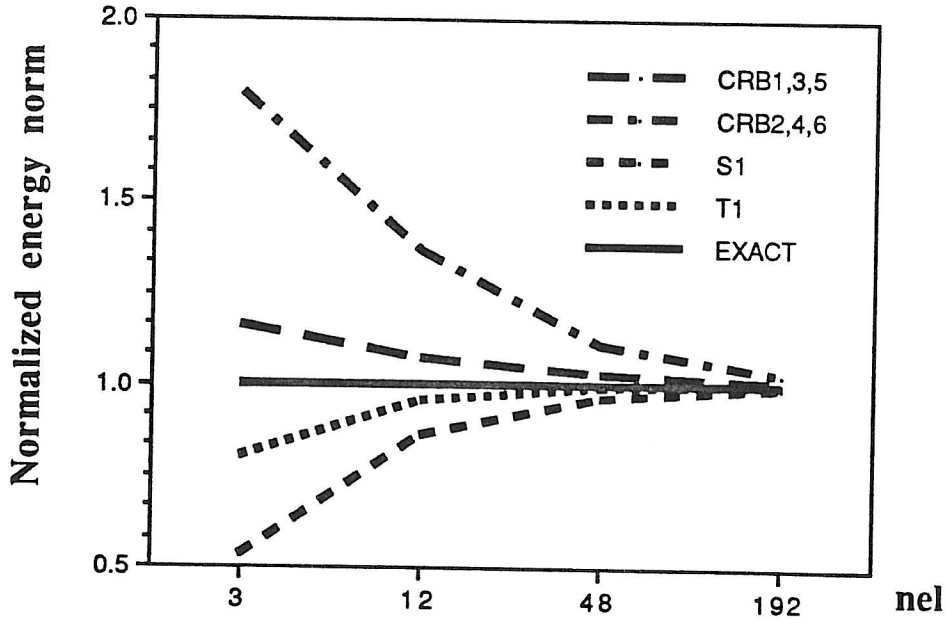

Figure 6.8: Clamped thin circular plate; uniform load; convergence in the energy norm.

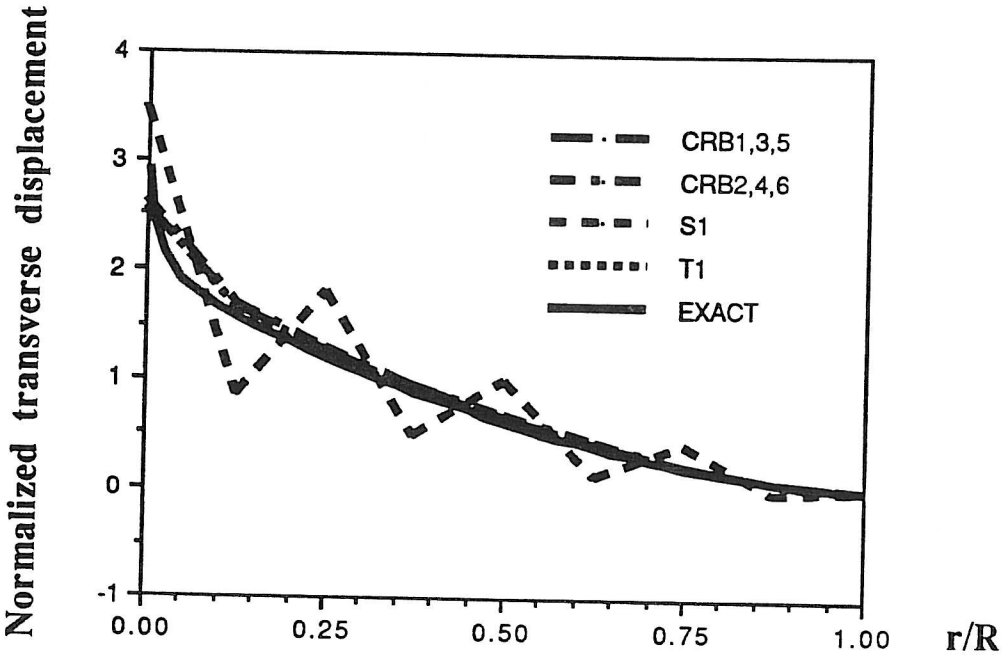

Figure 6.9: Clamped thick plate; concentrated unit load at the center; normalized transverse displacement along the radius.

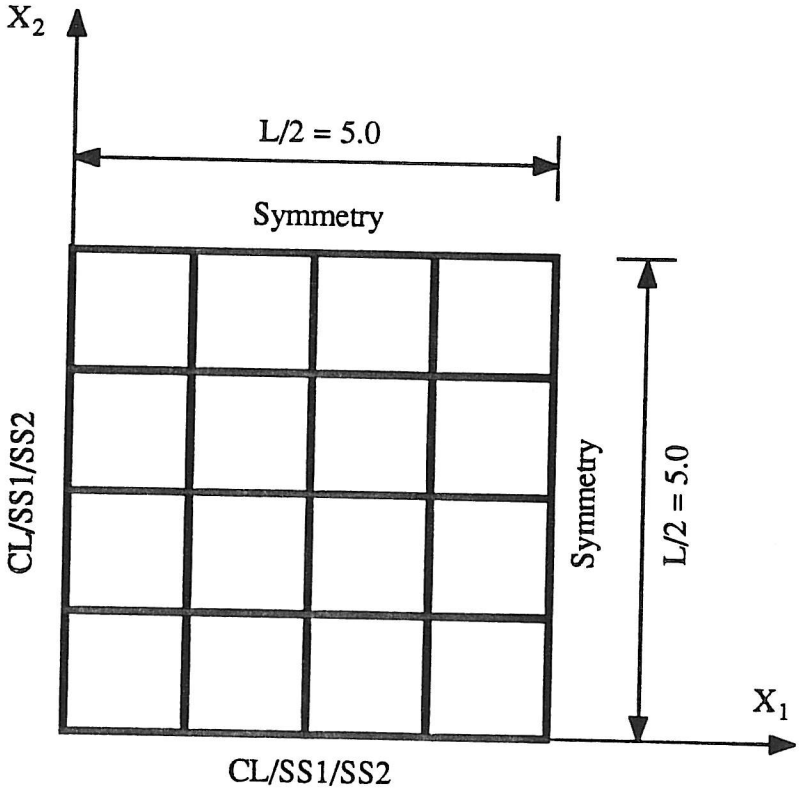

Figure 6.10: Square plate. Due to symmetry, only one quadrant is discretized.

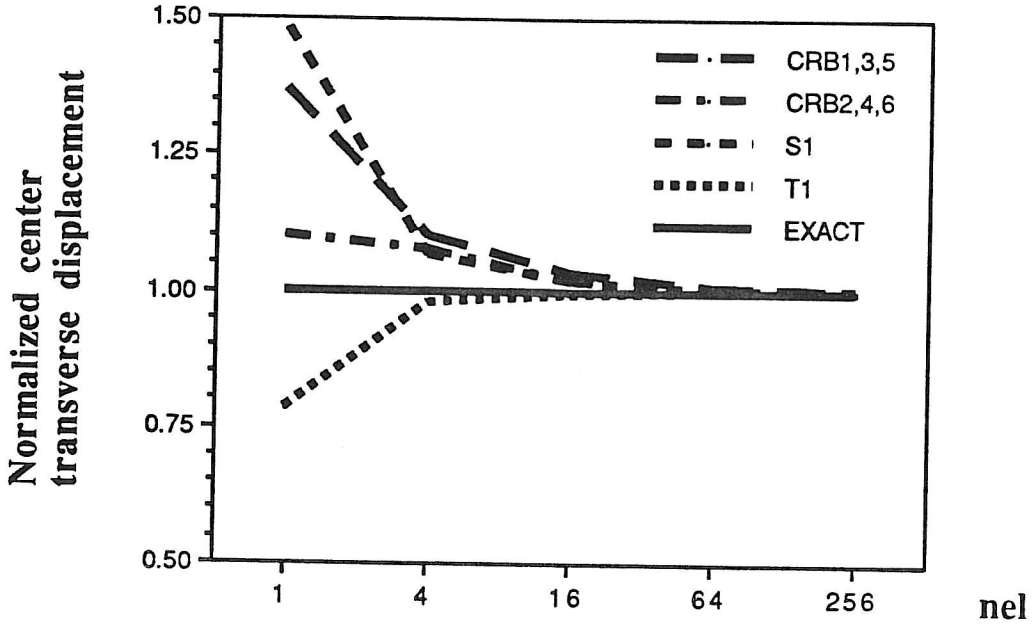

Figure 6.11: Simply supported (SS1) thin square plate; uniform load; convergence of the center transverse displacement.

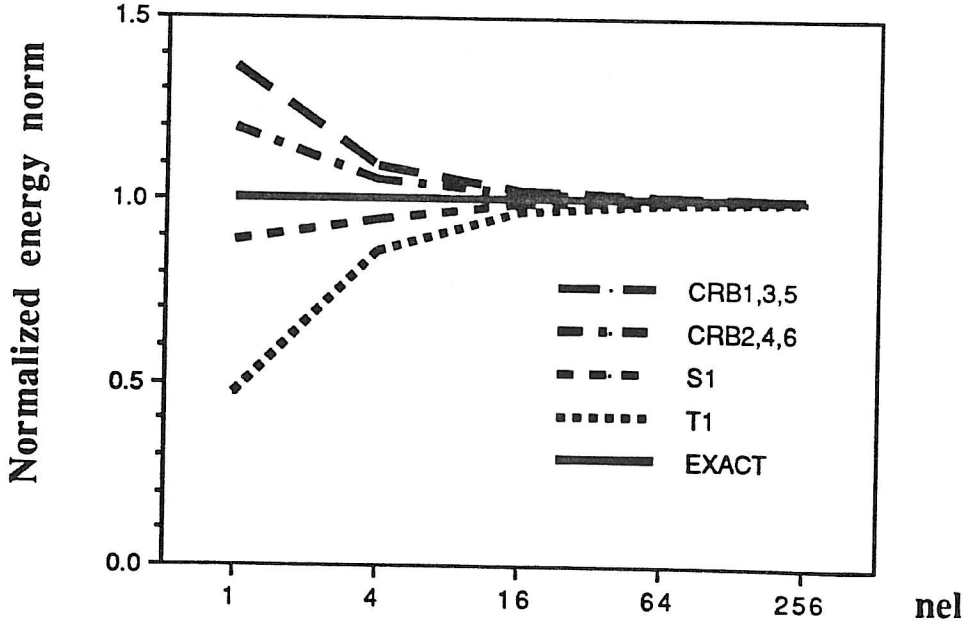

Figure 6.12: Simply supported (SS1) thin square plate; uniform load; convergence in the energy norm.

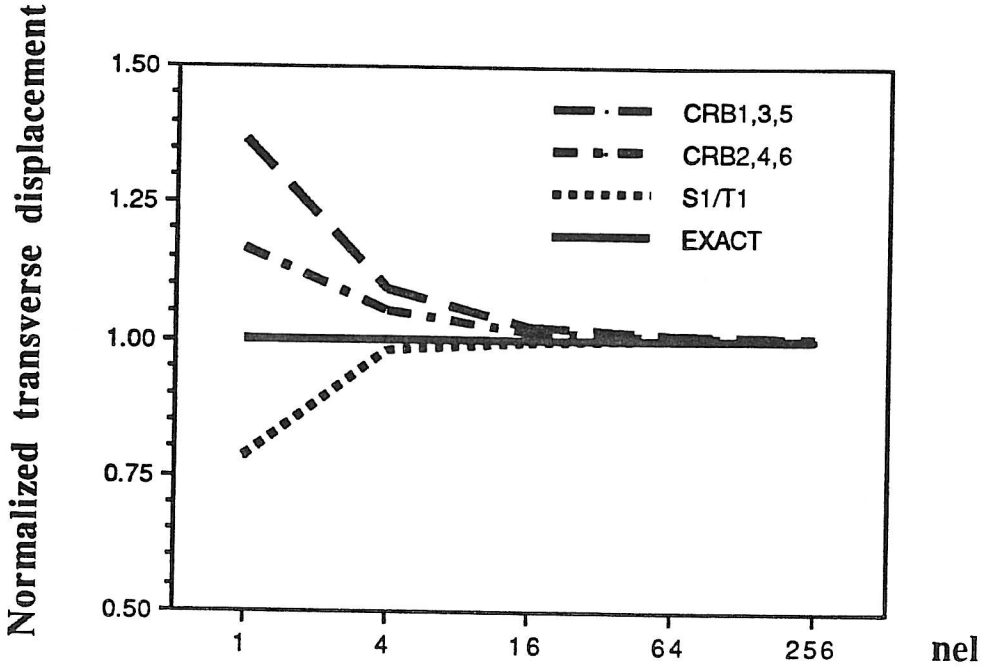

Figure 6.13: Simply supported (SS2) thin square plate; uniform load; convergence of the center transverse displacement.

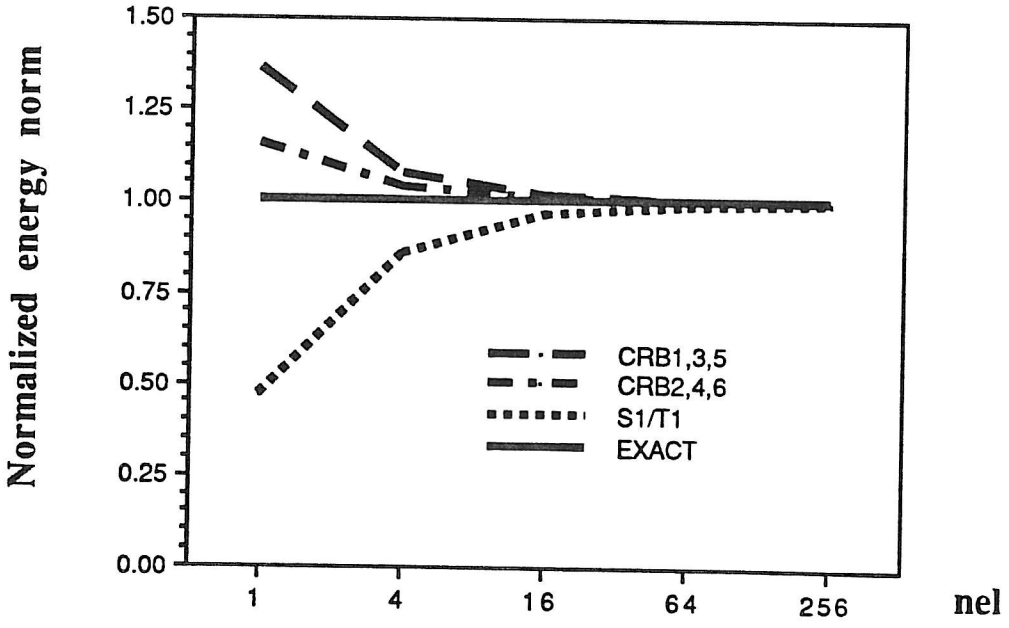

Figure 6.14: Simply supported (SS2) thin square plate; uniform load; convergence in the energy norm.

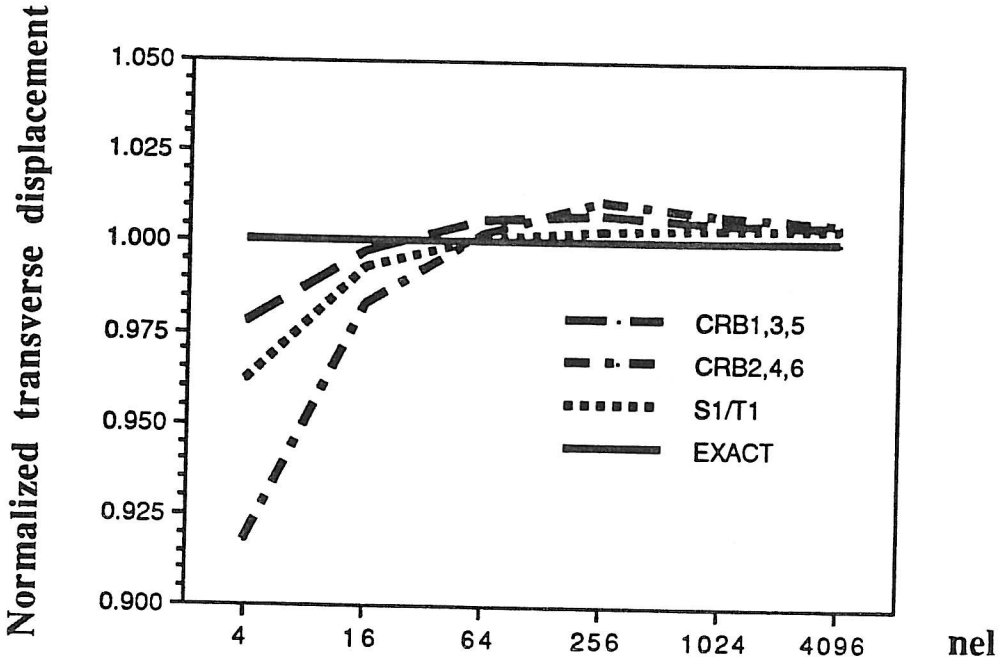

Figure 6.15: Clamped thin square plate; uniform load; convergence in the center transverse displacement.

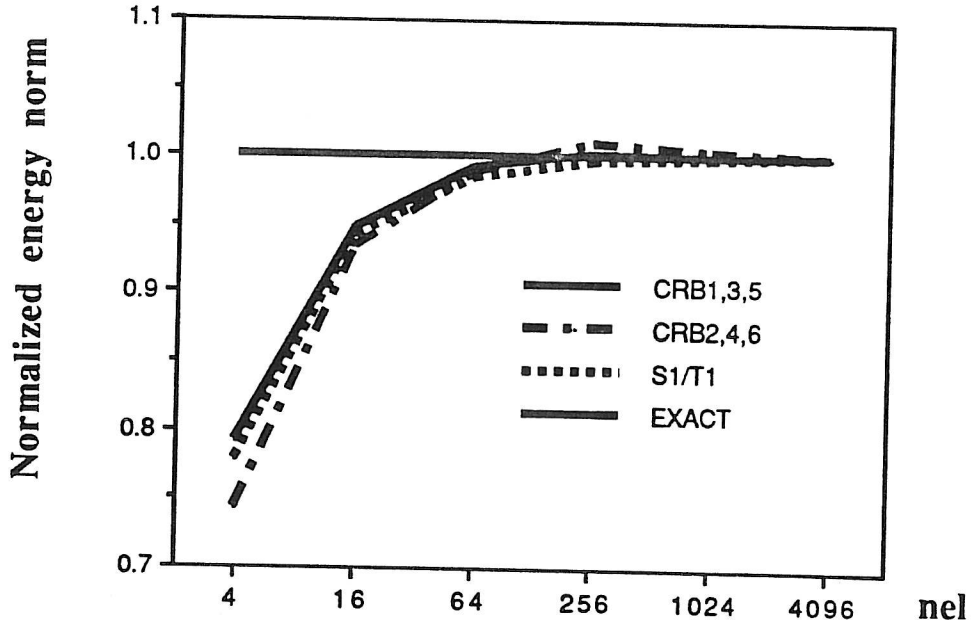

Figure 6.16: Clamped thin square plate; uniform load; convergence in the energy norm.

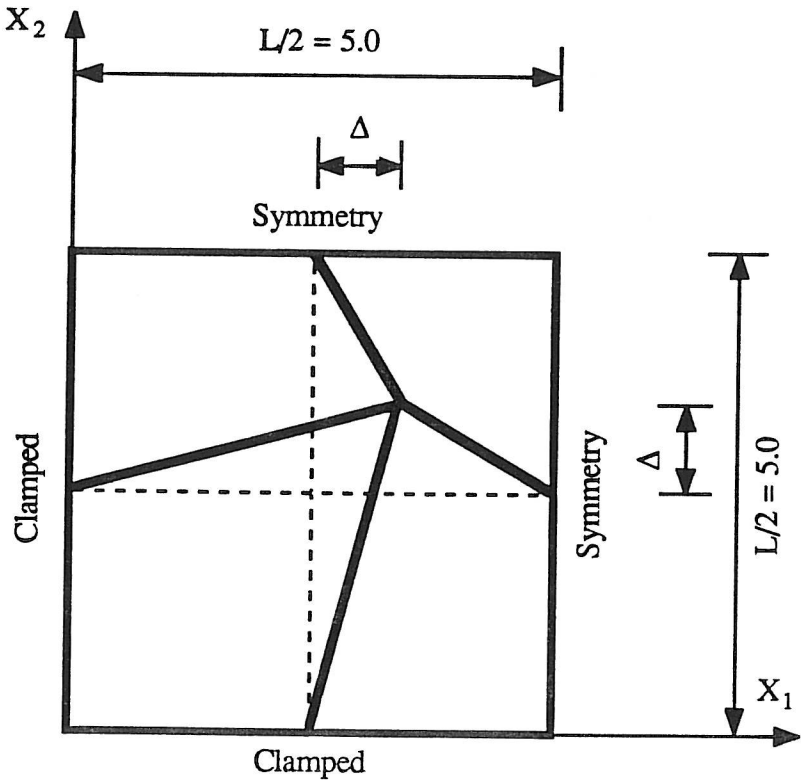

Figure 6.17: Mesh distortion; symmetric.

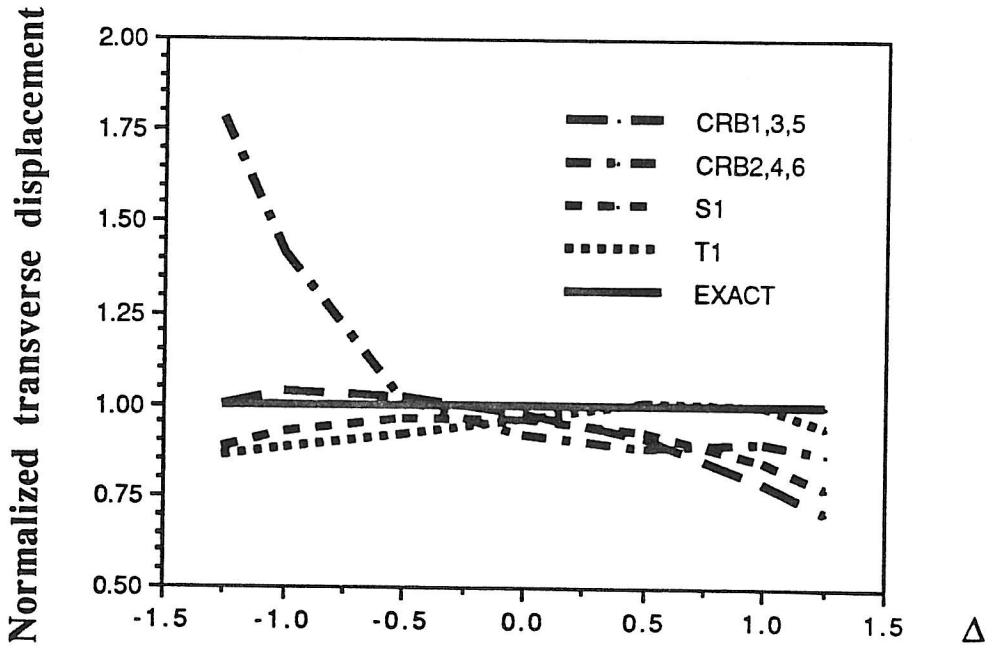

Figure 6.18: Sensitivity to mesh distortion; symmetric distortion; normalized center transverse displacement.

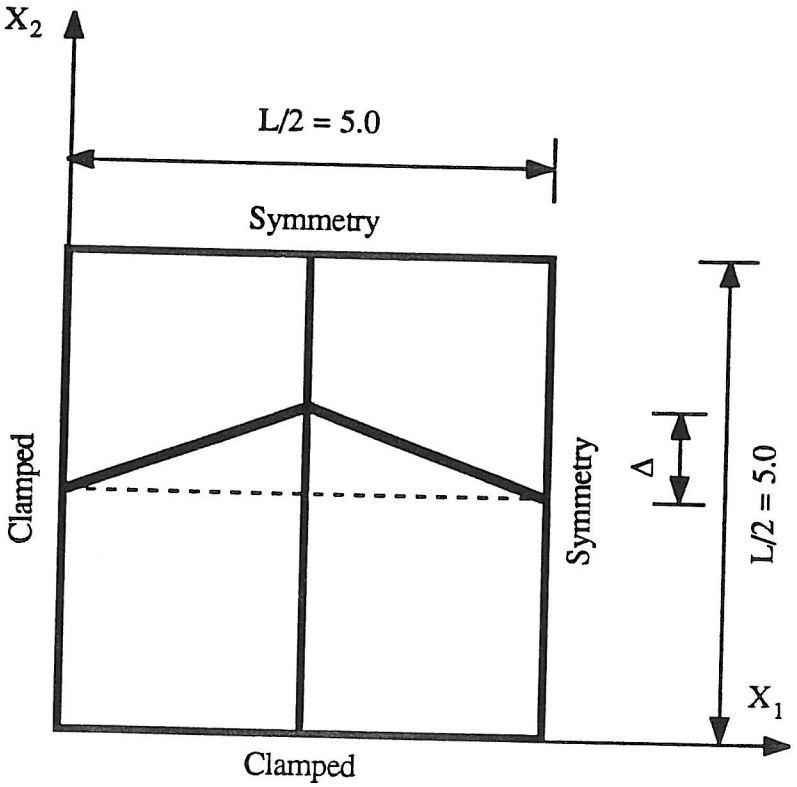

Figure 6.19: Mesh distortion; asymmetric.

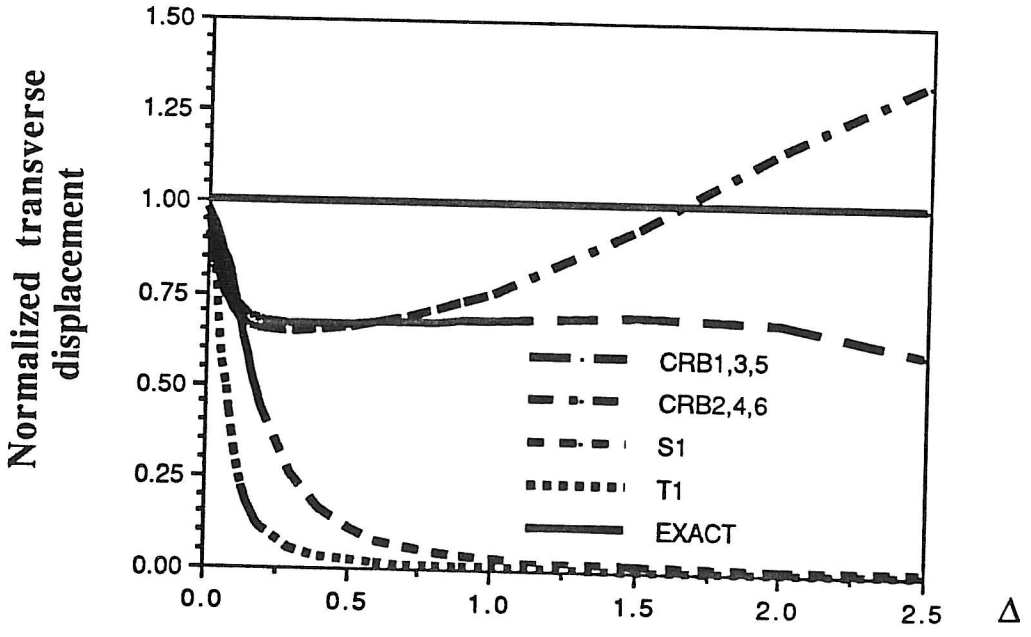

Figure 6.20: Sensitivity to mesh distortion; asymmetric distortion; normalized center transverse displacement.

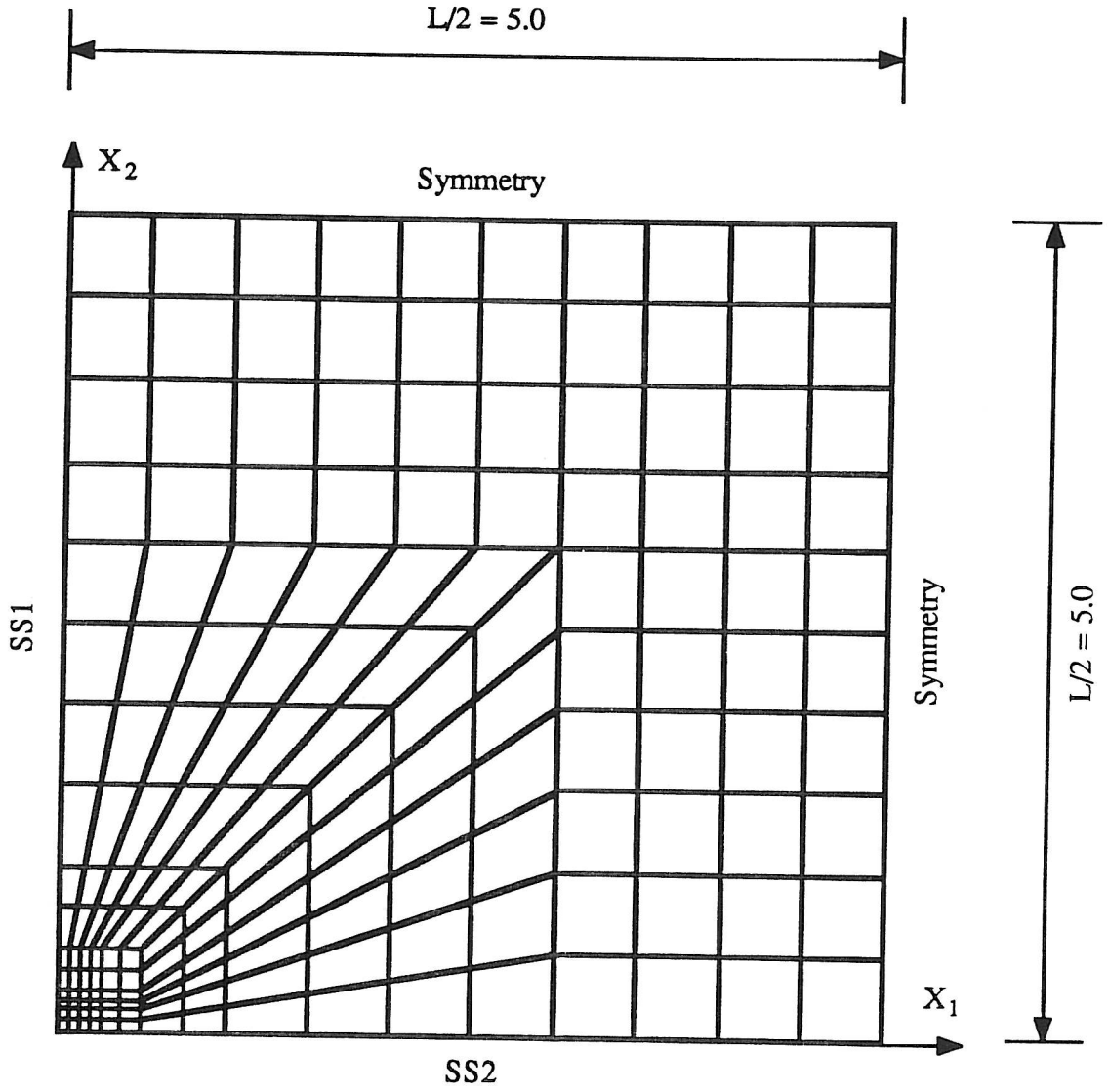

Figure 6.21: Square plate; graded mesh.

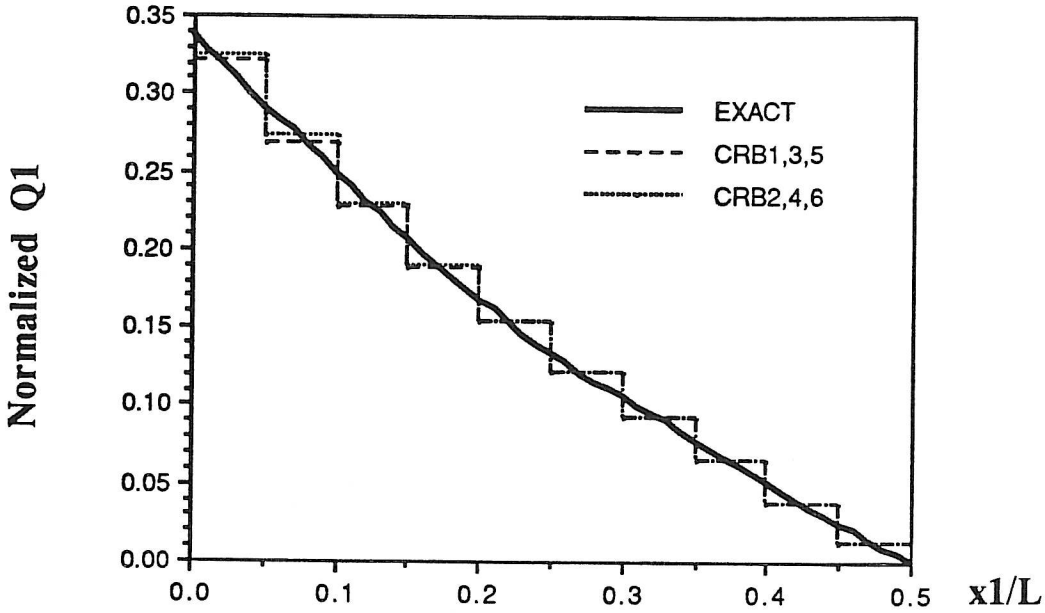

Figure 6.22: Variation of Q_1 along the line $X_2 = L/2$ for the uniformly loaded square plate with SS1/SS2 boundary conditions.

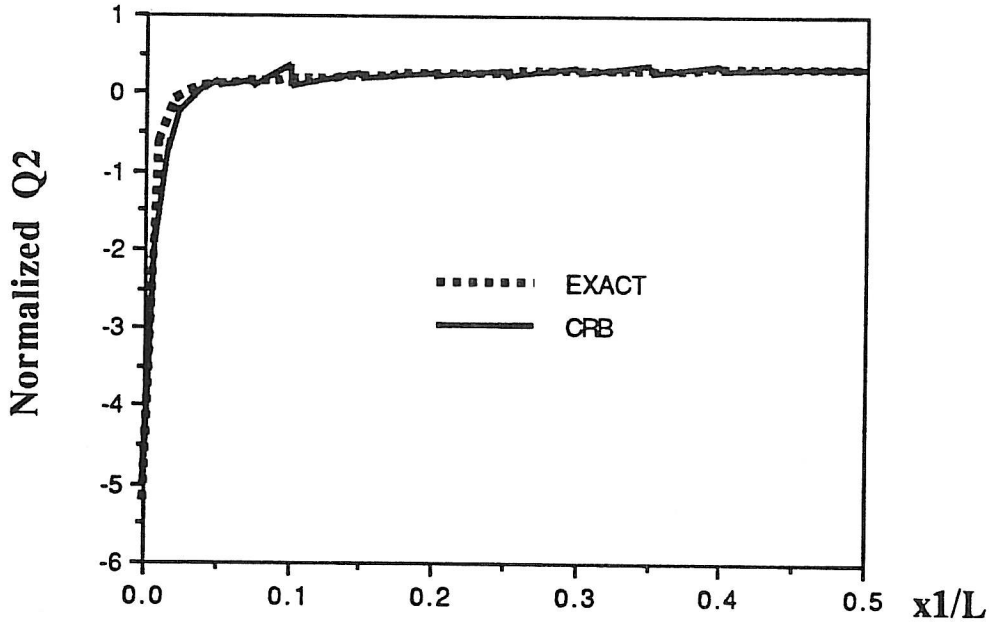

Figure 6.23: Variation of Q_2 along the line $X_2 = 0$ for the uniformly loaded square plate with SS1/SS2 boundary conditions; all CRB elements.

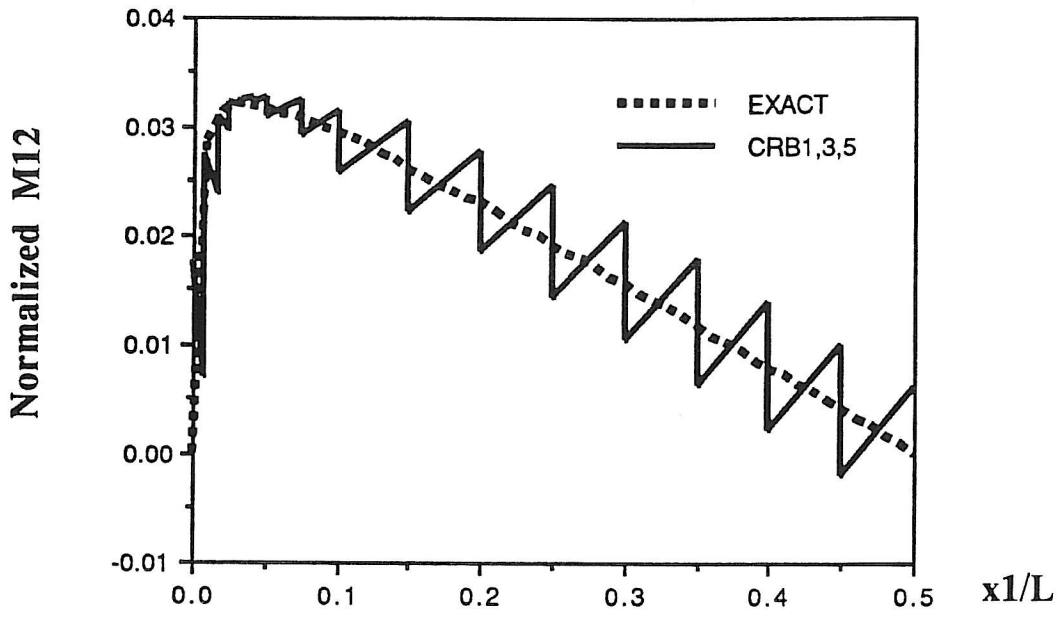

Figure 6.24: Variation of M_{12} along the line $X_2 = 0$ for the uniformly loaded square plate with SS1/SS2 boundary conditions; CRB1,3,5 elements.

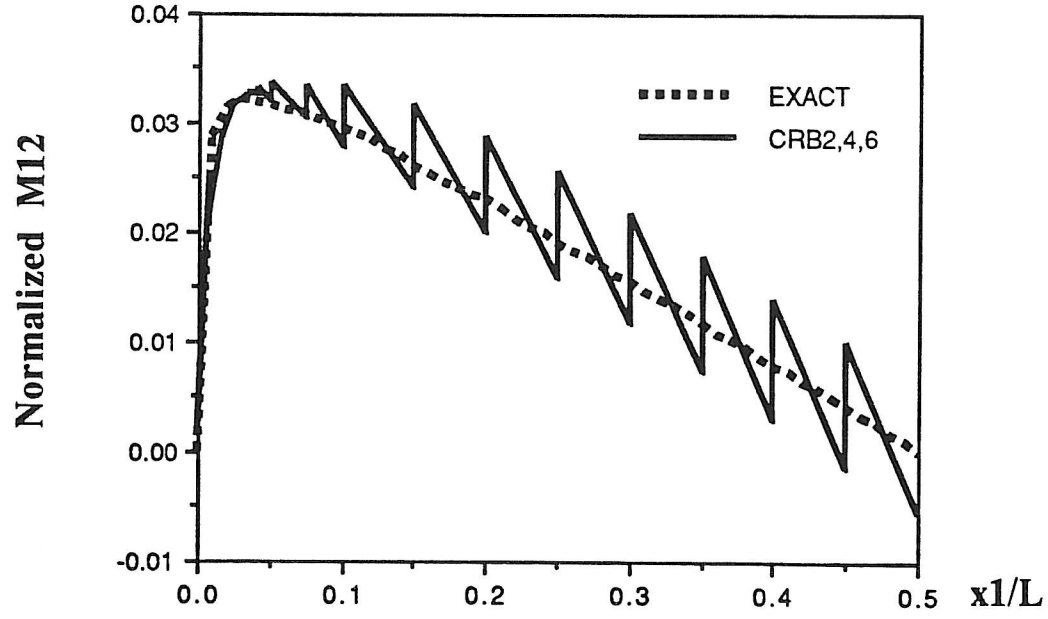

Figure 6.25: Variation of M_{12} along the line $X_2 = 0$ for the uniformly loaded square plate with SS1/SS2 boundary conditions; CRB2,4,6 elements.

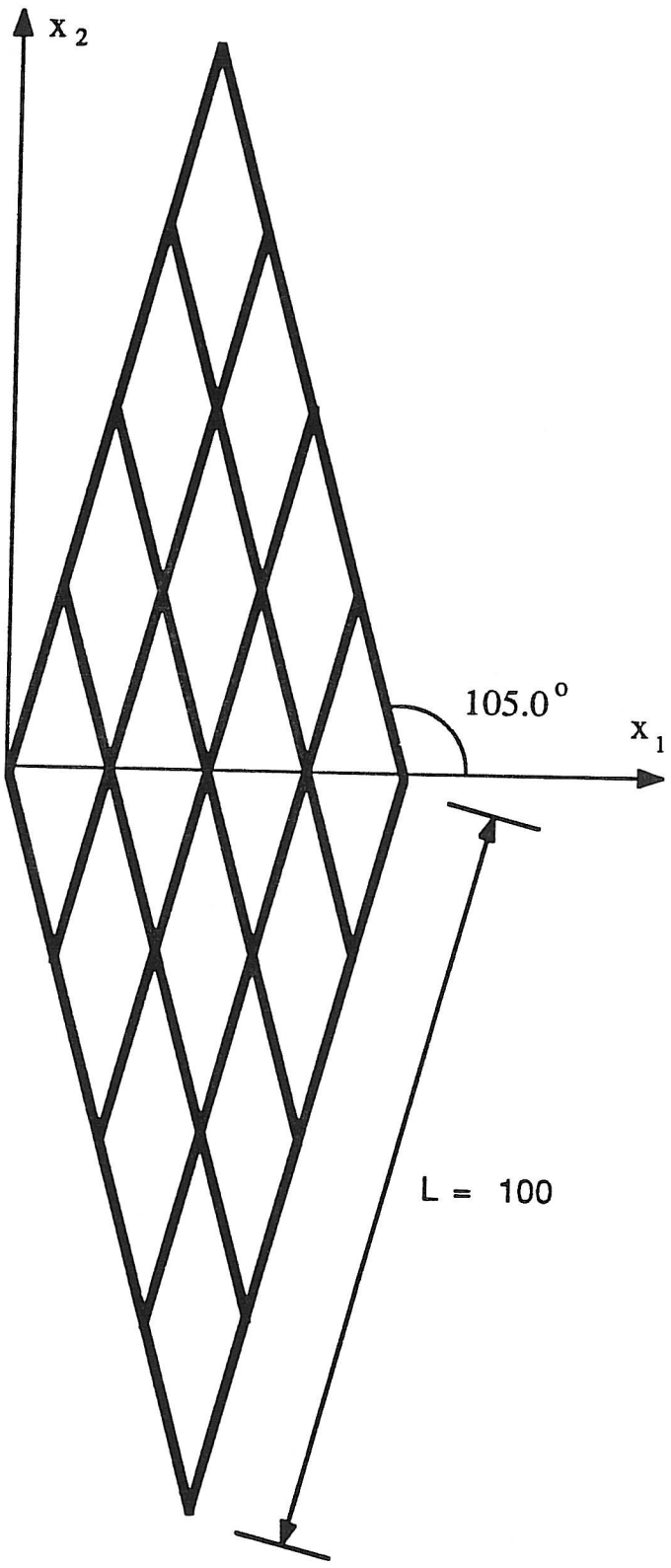

Figure 6.26: Rhombic plate mesh.

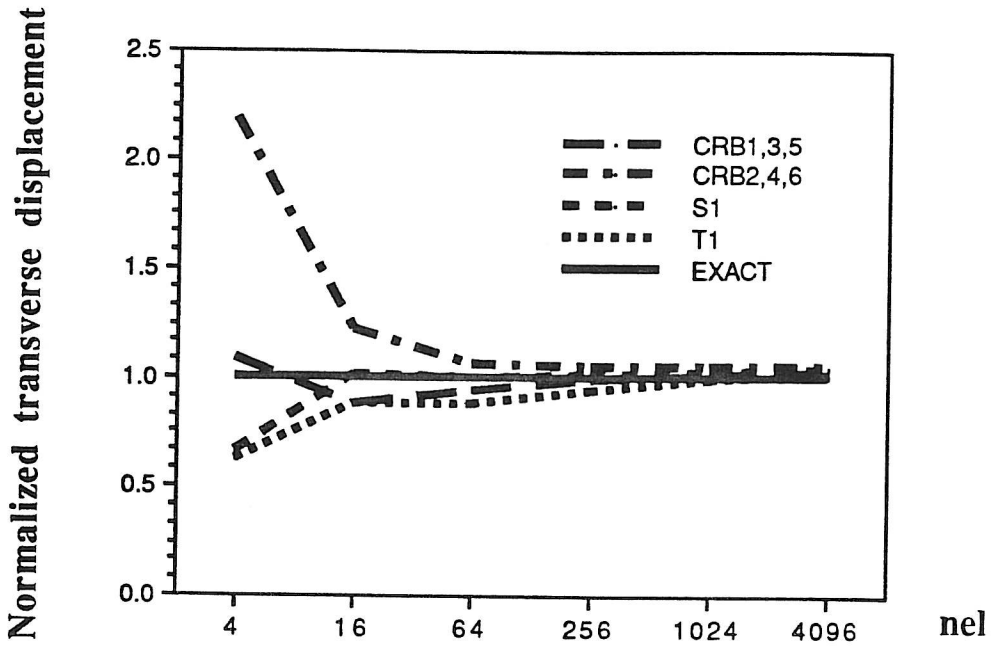

Figure 6.27: Rhombic plate; h = 1.0; convergence of the center displacement.

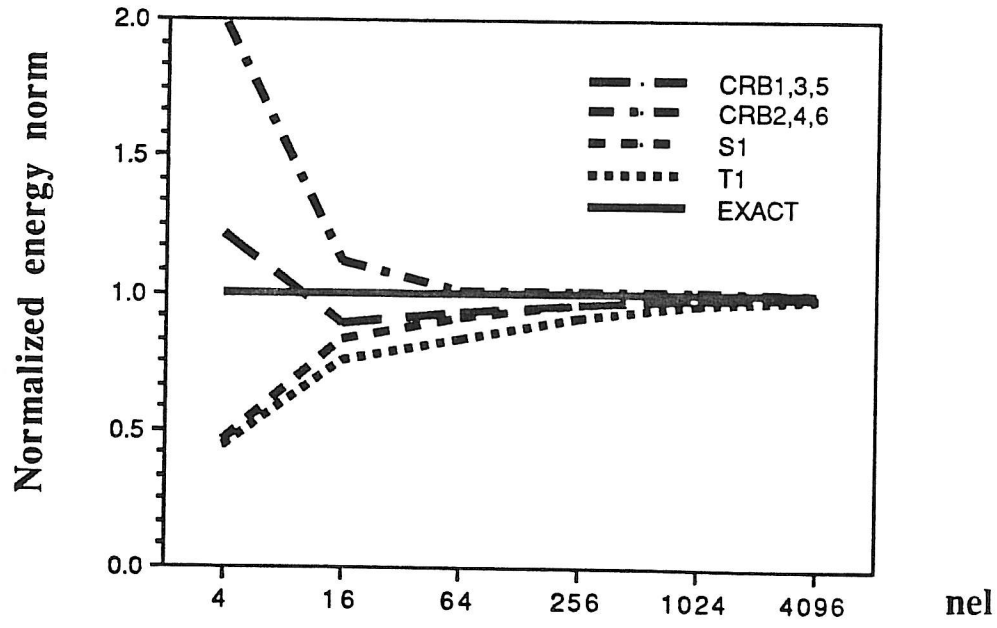

Figure 6.28: Rhombic plate; h = 1.0; convergence in the energy norm.

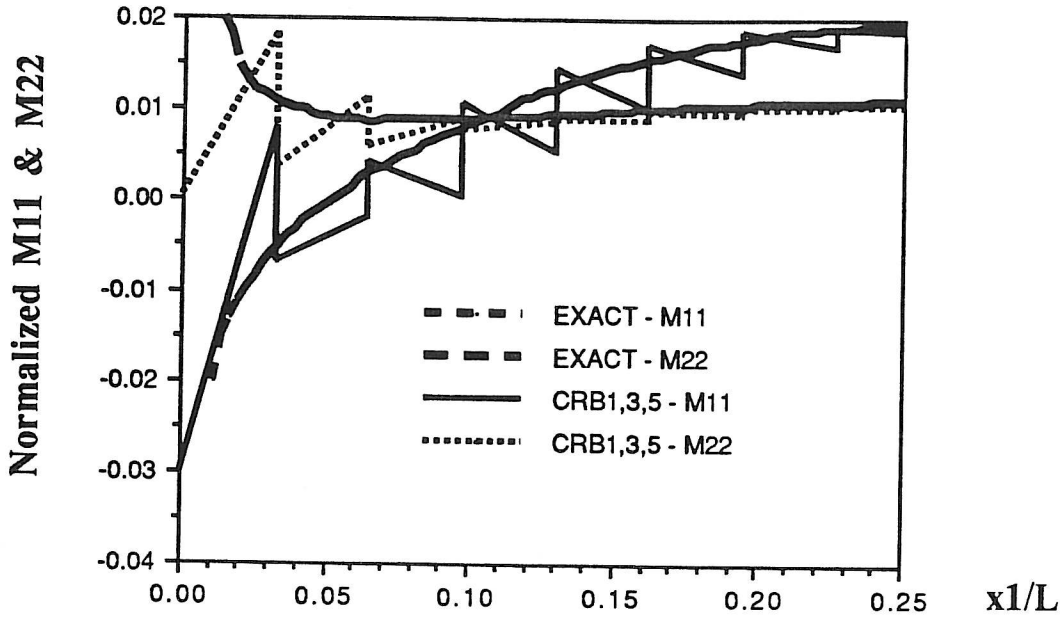

Figure 6.29: Rhombic plate; h = 1.o; variation of M_{11} and M_{22} along the line $X_2 = 0$; CRB1,3,5 elements.

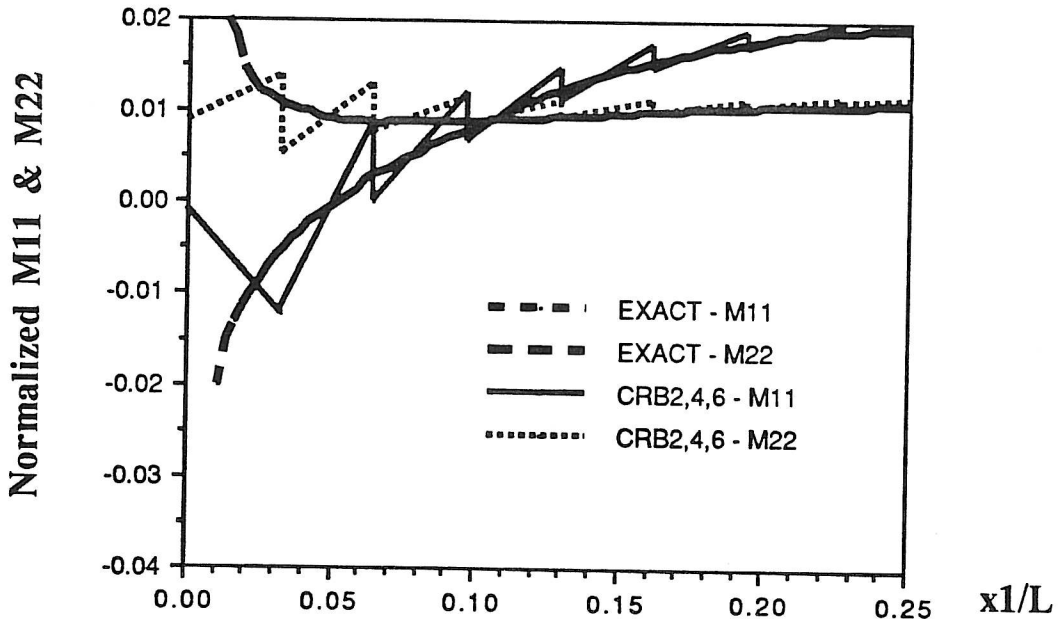

Figure 6.30: Rhombic plate; h = 1.0; variation of M_{11} and M_{22} along the line $X_2 = 0$; CRB2,4,6 elements.